Forschungszentrum Karlsruhe
Technik und Umwelt

Wissenschaftliche Berichte
FZKA 6151

Experimental Investigations of the Time Structure of the EAS Muon Component

I. M. Brancus, R. Haeusler, A. F. Badea, H. Rebel, T. Antoni, W. D. Apel, K. Bekk, K. Bernlöhr, E. Bollmann, H. Bozdog, A. Chilingarian, K. Daumiller, P. Doll, J. Engler, F. Feßler, M. Föller, H. J. Gils, R. Glasstetter, W. Hafemann, A. Haungs, D. Heck, T. Holst, J. Hörandel, K. H. Kampert, H. Keim, J. Kempa, H. O. Klages, J. Knapp, H. J. Mathes, H. J. Mayer, J. Milke, D. Mühlenberg, J. Oehlschläger, M. Petcu, U. Raidt, M. Risse, M. Roth, G. Schatz, H. Schieler, F. K. Schmidt, T. Thouw, H. Ulrich, J. Unger, B. Vulpescu, J. H. Weber, J. Wentz, T. Wibig, T. Wiegert, D. Wochele, J. Wochele, J. Zabierowski, S. Zagromski

Institut für Kernphysik

November 1998

FORSCHUNGSZENTRUM KARLSRUHE
Technik und Umwelt

Wissenschaftliche Berichte
FZKA 6151

Experimental Investigations of the Time Structure of the EAS Muon Component

I.M. Brancus[1], R. Haeusler, A.F. Badea[1], H. Rebel, T. Antoni, W.D. Apel, K. Bekk, K. Bernlöhr, E. Bollmann, H. Bozdog[1], A. Chilingarian[2], K. Daumiller[3], P. Doll, J. Engler, F. Feßler, M. Föller, H.J. Gils, R. Glasstetter, W. Hafemann, A. Haungs, D. Heck, T. Holst, J. Hörandel, K.H. Kampert[3], H. Keim, J. Kempa[4], H.O. Klages, J. Knapp[3*], H.J. Mathes, H.J. Mayer, J. Milke, D. Mühlenberg, J. Oehlschläger, M. Petcu[1], U. Raidt, M. Risse, M. Roth, G. Schatz, H. Schieler, F.K. Schmidt[3], T. Thouw, H. Ulrich, J. Unger, B. Vulpescu[1], J.H. Weber, J. Wentz, T. Wibig[4], T. Wiegert, D. Wochele, J. Wochele, J. Zabierowski[5], S. Zagromski

Institut für Kernphysik

[1] National Institute of Physics and Nuclear Engineering, Bucharest, Romania
[2]Cosmic Ray Division, Yerevan Physics Institute, Yerevan, Armenia
[3]Institut für Experimentelle Kernphysik, Univ. Karlsruhe, Germany
[4]Department of Experimental Physics, Univ. Lodz, Poland
[5]Soltan Institute for Nuclear Studies, Lodz, Poland
*Permanent address: University of Leeds, Leeds, U.K.

Forschungszentrum Karlsruhe GmbH, Karlsruhe
1998

Als Manuskript gedruckt

Forschungszentrum Karlsruhe GmbH
Postfach 3640, 76021 Karlsruhe

Mitglied der Hermann von Helmholtz-Gemeinschaft
Deutscher Forschungszentren (HGF)

ISSN 0947-8620

Abstract

The time structure of the Extended Air Shower (EAS) muon component, rather directly mapping the longitudinal shower development, is studied at sea level by measurements of the muon arrival time distributions using the muon detection facilities of the KASCADE central detector. Data have been analysed for EAS core distances up to 130 m for primary energies of the knee region. Results are presented for the distributions of various moments and the dispersion of the arrival times relative to the arrival time of the foremost muon, respectively. For the muon observations at larger core distances particular studies could be performed with the question to which extent EAS muon arrival time distributions display features with information about the mass composition of the primary cosmic rays. The present exploratory attempt is based on Linsley's approach of an indirect determination of the elongation rate and of the fluctuations of the height of the shower maximum.

Experimentelle Untersuchungen der Zeitstruktur der Myonkomponente ausgedehnter Luftschauer

Die Zeitstruktur der Myonkomponente ausgedehnter Luftschauer (EAS), die ziemlich direkt die longitudinale Schauer-Entwicklung abbildet, wurde mit Messungen der Myon-Ankunftszeitverteilungen auf Meereshöhe untersucht. Dabei werden die Myon-Nachweisanordnungen des Zentraldetektors des KASCADE-Experimentes benutzt. Die Meßdaten wurden bis zu Abständen von 130 m zum EAS-Kern und für Primärenergien der „Knie"-Region analysiert. Es werden Ergebnisse berichtet über die Verteilungen verschiedener Momente und der Streuung der Ankunftszeiten relativ zur Ankunftszeit des ersten Myons, sowie deren Variation mit dem Zenitwinkel der Schauereinfallsrichtung und mit der zur Energie nahezu proportionalen Myonzahl N_μ^{tr}. Für die Myonbetrachtungen bei den größten Abständen vom Schauerkern konnte eine spezielle Untersuchung mit der Frage durchgeführt werden, inwieweit EAS Myon-Ankunftszeitverteilungen Charakteristika zeigen, die auf eine Änderung der Massenzusammensetzung der primären kosmischen Strahlung im Energiebereich des „Knies" hinweisen. Der exploratorische Versuch basiert auf der Methode von Linsley für eine indirekte Bestimmung der Elongationsrate und der Fluktuationen der atmosphärischen Höhe des Schauermaximums.

Quid est ergo tempus ?
Si nemo ex me quaerat, scio;
si quaerendi explicare velim,
nescio.

Aurelius Augustinus (354-430 p. Ch. n.)

1 Introduction

The particles of Extended Air Showers (EAS) move nearly in the direction of the primary particle with velocities close to the velocity of light. Transverse moments and multiple scattering in the air produce a lateral dispersion. Differences in the velocities ("Lorentz effects") and, in particular, in the path-length, when travelling through the atmosphere, are the origin of a longitudinal dispersion of the EAS disc. This dispersion, i.e. the thickness of the shower disc, is reflected by the variation of the arrival times for particles, observed at a particular fixed location of the EAS lateral extension, as well as for particles of the extreme front (approximately represented by the relative arrival time of the first particle), observed at different distances from the shower centre. In the latter case the relative arrival times reflect the shape (curvature) of the EAS front and the direction of the EAS incidence.
Linsley and Scarsi [1] and Thielert and Wiedecke [2] did systematically explore the lateral dependence of the shower thickness, expressed by the median delay time as compared to the arrival time of the shower core. The increase of the time dispersion with the distance from the shower centre has been revealed. Since these early studies the time structure of the EAS charged particle component has been experimentally studied under various aspects. Most recently Agnetta et al. [3] and Ambrosio et al. [4] presented detailed results about various dependencies of the temporal structure of EAS charged particles based on measurements with the GREX/COVER-PLASTEX setup [3].
Simple kinematical arguments (see e.g. ref. [5, 6]) have been discussed that the time delay of the muon component carries some information about the height of production i.e. the longitudinal EAS profile, via time-of-flight effects. This feature arises from the fact that higher-energy muons above a few GeV travel through the atmosphere in a relatively undisturbed way. That aspect has been pursued by detailed investigations of the temporal structure of the muon component with the underground water-Cerenkov-detector setup of the Haverah Park [7], exploring the dependence of the time-delay from the inclination θ of the shower axis, from the primary energy E_0 (or shower sizes N_e and N_μ, respectively), and from the distance R_μ from the shower core. Walker and Watson [8] directed the interest to fluctuations, whose origin could be interpreted as fluctuations of the height of maximum of the shower development due to different masses of the primaries, as consequence of different interaction lengths of the primaries and the multiplicities, energy and momentum distributions of the secondaries (the parent particles of the muons) [9].
The interest of this specific kind of Extended Air Shower investigations is directed to

EAS observables which represent the arrival time distributions, i.e. the distributions of various characteristic moments Q_T like the mean values, median values of the single distributions etc. and their dispersions. The variation of these moments with the distance from the shower core R_μ is considered as representation of the EAS time profile [10]

$$Q_T(R_\mu) = F(R_\mu; E_0, M(N_e, N_\mu), \theta; E_{\text{thres}}, n, ...) \tag{1.1}$$

which is dependent from the energy E_0 and nature (mass M) of the primary particle (reflected by adequate shower variables like N_e, N_μ), from the angle θ of shower incidence and additionally from biasing trigger and observation conditions: energy threshold E_{thres} and multiplicity n of the muon detection.
The present paper reports about experimental studies of the time structure of the EAS muon component based on data measured with the KASCADE detector system [11]. The investigation tries to explore the phenomenological features, and it studies empirical parameterisations of the observed time profiles, rather than the specific sensitivity to the mass of the primary particles. However the experimental results could be compared with results of detailed EAS Monte-Carlo simulations, using the program CORSIKA [12] and taking into account the response and timing qualities of the detectors. Results of such an analysis will be communicated in a separate paper.

2 The timing and muon identification facilities of the KASCADE Central Detector

In the centre of the KASCADE field, covered by an array of 252 detector stations, measuring the EAS electron-photon and muon component with a threshold of 3 MeV and 300 MeV, respectively (for details see Ref. [11]), there is the KASCADE Central Detector (Fig. 1), which is composed of various different detector components. Basically the setup is an iron sampling calorimeter for the identification and energy measurement of hadrons, in particular in the shower core. The 8 active detector layers, measuring the energy loss of the traversing hadrons, are built up from room-temperature liquid (tetramethylsilan) ionisation chambers. In the basement of the setup, below 3800 t of iron and concrete, there is an installation of large-area position-sensitive multiwire proportional chambers (MWPC) for identification of muons of energies larger than 2 GeV, and exploiting the relatively good spatial resolution, for studies of the lateral distribution of particles penetrating through the absorber above, preferentially muons, but also the high energy tails of "punch-through" hadrons of the shower core (and secondaries) [13]. The MWPC system is arranged in double-layers with a telescope effect, improving the reconstruction quality of the particle hits and informing about the mean direction. One active layer of the calorimeter setup is a system of scintillation detectors for providing a fast trigger signal (in addition to the trigger from the field array) for the MWPC and for timing measurements. This timing layer is built up by 456 detector elements, covering effectively 64% of the total central detector area.

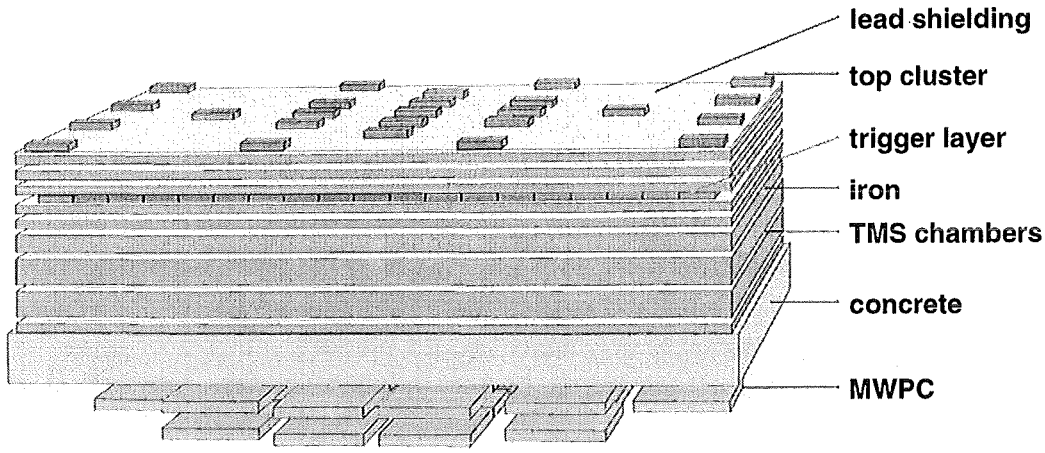

Figure 1: *The KASCADE Central Detector.*

Each single detector consists of two quadratic scintillator sheets of 3 cm thickness and 0.45 m^2 in area, with a readout by a wavelength shifter bar and a 1.5-inch photomultiplier. Two of these elements are housed, optically separated, in a tight detector box. The average time resolution is determined to 1.8 ns. In addition this detector layer is used in calorimetric mode as a muon detector ($E_{\mathrm{thres}} = 0.4$ GeV). By two different thresholds the electronic readout allows to discriminate the energy loss of minimal ionising particles and of hadrons (50 m.i.p.). The trigger and timing facility [14] (installed in the third gap from above) is shielded by lead and iron (c. 30 r.l.), so that the contribution of punch-through-events of the electromagnetic component to muons events, identified with the low-energy threshold, gets negligible in the range of distances of > 30 m from the shower centre. For studies of the higher-energy muons (> 2 GeV) the MWPC do filter this part efficiently. The top cluster is an array built up of 25 modules of the same type of detectors as used for the timing layer. It supplements the measurements of the charged particle density for determining the shower size, but can be used additionally for timing and trigger purposes. Thus, the KASCADE Central Detector system allows to study lateral and time distributions of the EAS muon component with two different energy thresholds. Additionally, in combination with the top cluster, arrival time differences between the electron-photon and the muon component are currently investigated [15].

3 Definitions of the observables and general procedures

The present investigation explores the temporal features of the muon component at energies above 2 GeV, measured as correlated signals of the trigger layer and the MWPC

chambers, and associated by the general KASCADE event trigger to an EAS event. The EAS event can be characterised by shower core position $R_{\rm cor}$ (measured from the centre of the central timing layer, e.g.), the direction of shower incidence (θ,Φ), by the shower size N_e, the muon number N_μ or the "truncated" muon number N_μ^{tr}, respectively. The quantity N_μ^{tr} is the muon content with $E_\mu > 250$ MeV, integrated in a limited range of 40 - 200 m from the centre of the lateral muon distribution. As Monte-Carlo simulations show [16], due to various fortunate features of the lateral distribution, $\log_{10} N_\mu^{tr}$ proves to be nearly proportional to $\log_{10} E_0$ and is almost independent from the primary mass for the KASCADE observation level. Thus a classification of the EAS by N_μ^{tr} can be regarded as an approximate energy classification. Therefore we prefer a classification by N_μ^{tr} instead of by the shower size N_e, which would prepare samples of mixed energies, dominated by the larger fluctuations of proton-induced showers (see ref. [13]). The reconstruction accuracy of N_e and N_μ^{tr} is estimated to be of the order of $10 - 20\%$, for the core location about 2 m for showers located within 100 m from the array centre, and for the angle-of-incidence of the shower about 0.5^o.

Measurements of the relative muon arrival times refer to an experimentally defined zero-time. In many studies the arrival time $T_{\rm cor}$ of the shower core is used as reference [5], [6], also in the first analysis of relative muon arrival times with KASCADE data [17], whereby the distributions of the arrival time of the foremost muon T_μ^1, of the mean T_μ of the single distributions, and the corresponding standard deviations σ have been regarded:

$$\Delta\tau_1^{glob} = T_\mu^1 - T_{\rm cor} \qquad \text{and} \tag{3.1}$$

$$\Delta\tau^{glob} = T_\mu - T_{\rm cor} \tag{3.2}$$

Time quantities referring to $T_{\rm cor}$ are furtheron called "global" times. Analysing the first measurements, it turned out [17] that $T_{\rm cor}$ is not well determined by the present reconstruction procedures from the arrival time of the electromagnetic component near the shower core, and it introduces an additional jitter of some nanoseconds. Thus, for many detailed considerations we prefer to analyse "local" times, which refer to the arrival of the foremost muon, registered in the timing detector at the particular distance from the centre R_μ ($= R_{\rm cor}$ in case of vertical showers, if we define the centre of the Central Detector as the origin of the coordinate system, used to specify a certain position in the KASCADE detector field):

$$\Delta\tau^{loc}(R_\mu) = T_\mu(R_\mu) - T_\mu^1(R_\mu) \tag{3.3}$$

(The label "loc" is furtheron omitted.)

In general, R_μ is defined in a plane perpendicular to the shower axis, which specified by zenith angle θ and the azimuth Φ of the direction of incidence.

For a detailed discussion of the time structure we introduce specific moments Q_T of the distributions: the *first quartile* ($\Delta\tau_{0.25}$) the *median value* ($\Delta\tau_{0.50}$) and the *third quartile* ($\Delta\tau_{0.75}$) which pronounce various different features of the distributions. Another question, independent of the reconstruction of the arrival time of the shower core is the reliability of the reconstruction of the *location* of the core. Studies have been made in this direction by Glasstetter et al. [18] reporting about misreconstructions of the core

location at distances $\geq$ 100 m. To which extent the misreconstructions do depend from the shower size and the direction of incidence has not been studied. In studies of muon arrival time distributions a specific interest is focused to the time structure just at large radii R_μ, since the path-length effects of the muon travel get more pronounced. Hence in a first step, we try to explore how far we could extend the reliable range of R_μ by an extrapolation under the condition of a regular continuation of the temporal shower profile. It should be noted that also the slope of the shower profile at small radii is also of actual interest for being used to define $T_{\rm cor}$ more accurately with an adequate reconstruction technique.

The experimental data were accumulated during 900 hours in the period of Sep. 30 to Dec. 3, 1997. The total number of collected events amounts to c. 200 000 with the requirement that at least 3 timing detectors of the timing facility of the central detector must have a correlated signal with the MWPC. In a first step these events have been scrutinised along the arrival times $\Delta\tau_1^{glob}$ of the first muon (relative to the *reconstructed* arrival time $T_{\rm cor}$ of the shower core) as a function of the distance R_μ from the reconstructed shower centre (see appendix A). For $R_{\rm cor} \leq 100$ m the values of $\Delta\tau_1^{glob}$ are concentrated in a time band of about 40 ns. Only extremely seldom there are events with first muons of larger delays. For the present analysis of the average features of time dispersion of the EAS muon component, we may ignore such events. For $R_{\rm cor} > 100$ m, i.e. for shower cores located outside the KASCADE array, one observes a conspicuous increase of seemingly delayed events extending the 40 ns - band. Though the origin of these events is finally not clear, we ascribe the effect to problems of the shower reconstruction procedures for large $R_{\rm cor}$, and these events have been discarded from the sample to be analysed. Nevertheless the fraction of these events is smaller than c. 0.5%

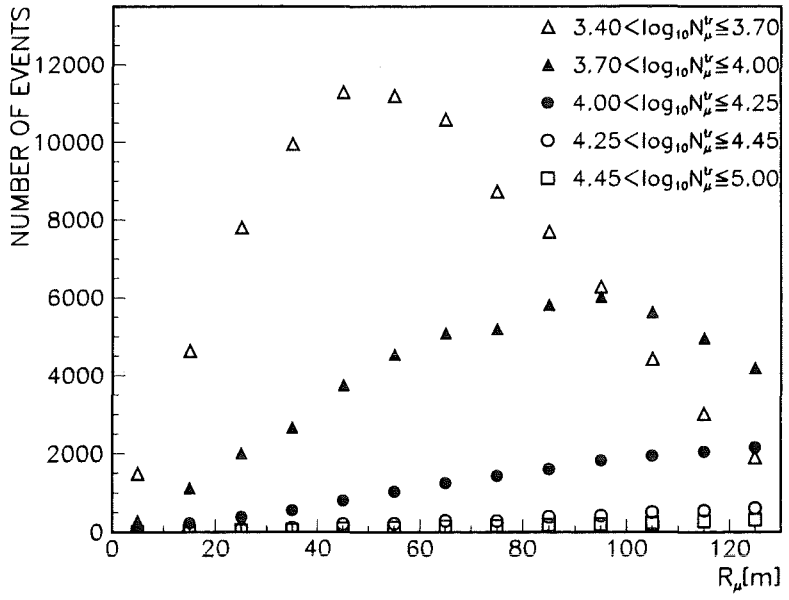

Figure 2: *Event distribution of the analysed sample along the shower core distances.*

for $R_{\rm cor} \leq 130$ m. When analysing the radial dependence of the EAS time structure up to $R_\mu = 130$ m, the events located at larger radial distances, - selected within the $\Delta\tau_1^{glob} = 40$ ns band, *but signalled by at least 3 muons in the timing detectors* - behave quite normally and continue monotonically the trend from the smaller R_μ values. This is corroborated by studies comparing large R_μ shower events with cores located in different azimuthal directions of the KASCADE array (see appendix A). Thus we conclude that with the applied conditions the investigations of EAS observed by KASCADE could be safely extended to core distances at least up to 130 m. Figure 2 shows the distribution (averaged over all zenith angles) of the core locations for different ranges of N_μ^{tr} in the sample under consideration. It should be noted that the condition limiting $\Delta\tau_1^{glob}$ to 40 ns, does not imply that the (local) arrival time distributions relative to $T_\mu^1(R_\mu)$ are restricted to that range. For the analysis of the single distributions $T_\mu(R_\mu) - T_\mu^1(R_\mu) \leq 500$ ns is accepted.

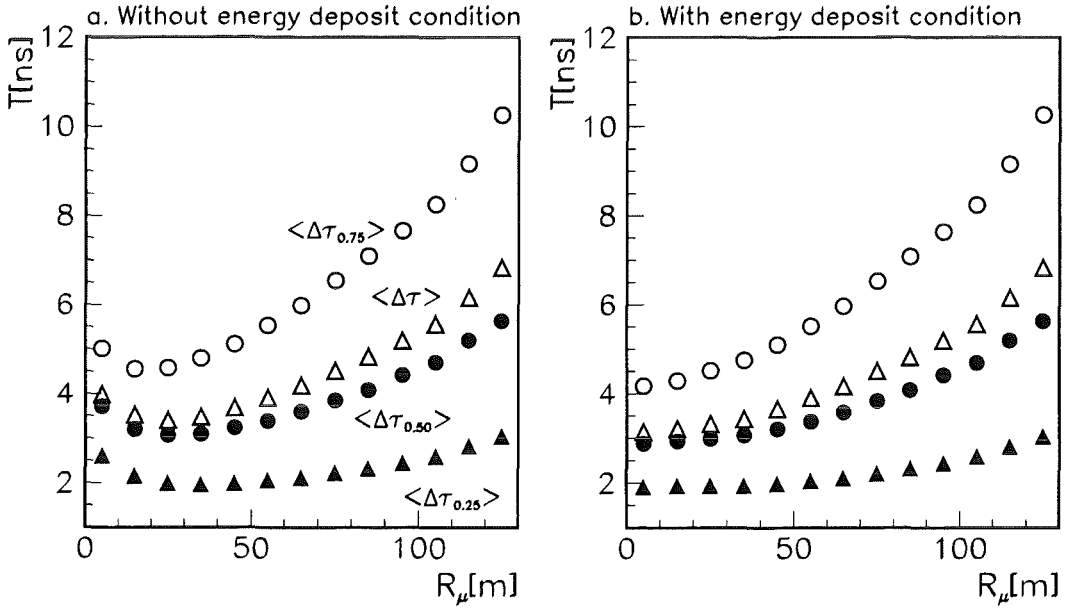

Figure 3: *The radial dependence of the averaged (local) mean $\Delta\tau$, the median $\Delta\tau_{0.50}$ and the quartiles $\Delta\tau_{0.25}$ and $\Delta\tau_{0.75}$ (averaged over all shower sizes): a. without condition for the energy deposit E_{dep} in the timing detectors. b. with the condition $E_{dep} \leq 20$ MeV.*

Measurements of the muon component at small core distances ($R_\mu < 30$ m) are usually affected by the electromagnetic punch-through and by the hadrons in the shower core. Due to the identification of the 2 GeV muons by the MWPC positioned under the iron calorimeter, the disturbance by electromagnetic punch-through can be excluded. However, hadrons inducing in the timing detectors shower events with high-energy secondary muons, fake systematically early "first muons", which distort the relative arrival time distributions. Figure 3 displays this effect for the means of the (local) mean $\Delta\tau$, the

median $\Delta\tau_{0.50}$ and the quartiles $\Delta\tau_{0.25}$ and $\Delta\tau_{0.75}$ distributions (averaged over all shower sizes and N_μ^{tr}, respectively and called furtheron averaged shower profile, see sect. 4). In order to suppress faked muons from hadrons , the condition of an energy deposit in the scintillator detectors $E_{dep} \leq 20$ MeV (c. 3 m.i.p.) has been applied, which remedies the distortion effect (see Figure 3).

4 The EAS muon shower profile

We consider the muon arrival time distributions in different intervals of the core distance R_μ = 10 - 20 m ..... up to 130 m (in some cases, for sake of statistical accuracy, also comprised to larger ΔR_μ- bins), for different ranges of the zenith angle of shower incidence and for 5 different ranges of $\log_{10} N_\mu^{tr}$ (see Figure 2). From the local arrival time distributions of the single shower events we derive the distributions of various moments, of *the mean* $\Delta\tau$, *the median* $\Delta\tau_{0.50}$, the *first* $\Delta\tau_{0.25}$ and *third* $\Delta\tau_{0.75}$ *quartiles.* Examples of such distributions for different moments and different $\log_{10} N_\mu^{tr}$ ranges are shown in Figures 4 and 5, respectively.

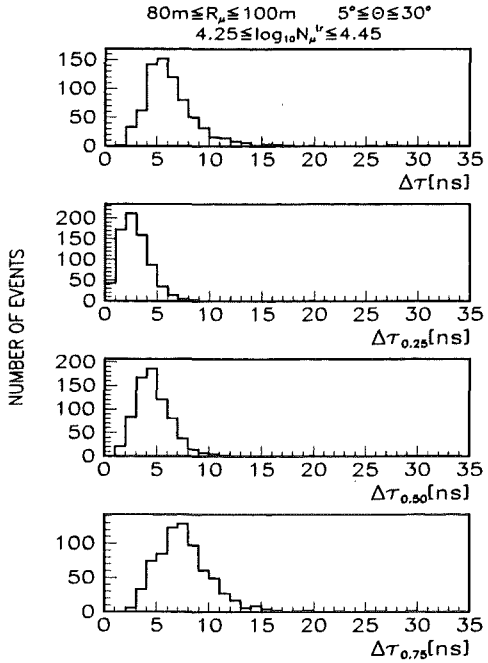

Figure 4: *The distribution of various different moments of the experimental muon arrival time distributions observed in a particular interval of the distance from the shower centre and for a particular* $\log_{10} N_\mu^{tr}$ *range.*

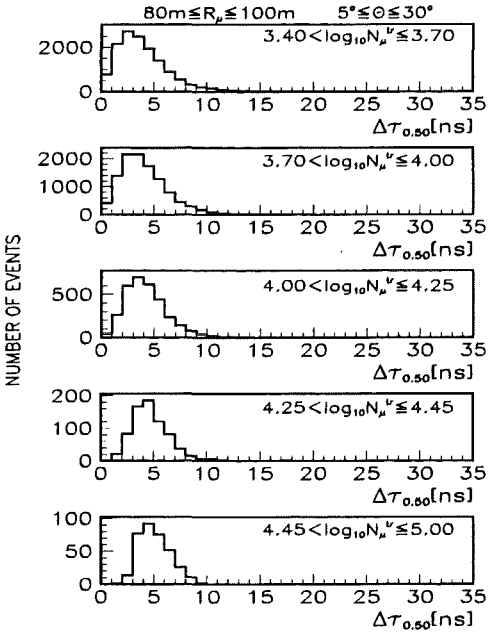

Figure 5: *The distribution of the median values of the muon arrival time distributions observed for different* $\log_{10} N_\mu^{tr}$ *ranges in a particular interval of the distance from the shower centre.*

These results have been further processed by determining the mean values and the variances σ^2 (standard deviations σ) of *the mean* $\Delta\tau$, *the median* $\Delta\tau_{0.50}$, *of the quartiles* $\Delta\tau_{0.25}$ and $\Delta\tau_{0.75}$ distribution. Their R_μ-dependence displays the *muon profile* of the EAS disc in a comprised and representative way.

4.1 Averaged profiles

Figures 6 and 7 display the variation of the averaged distributions of the median and of the quartiles $\Delta\tau_{0.25}$ and $\Delta\tau_{0.75}$ of the muon arrival time distributions with the distance from the shower core, (integrated over the observed size spectrum). In studies of the charged-particle EAS component it has become customary to parameterise the observed distributions by a Γ-probability distribution function [19, 20, 3] , given by

$$\Gamma(Q_T) \;=\; a\, Q_T^b exp(-c\, Q_T) \tag{4.1}$$

with a mean value $T(R_\mu) \;= < Q_T > = \; (1+b)/c$ and the standard deviation $\sigma^\Gamma = (1+b)^{1/2}/c$.

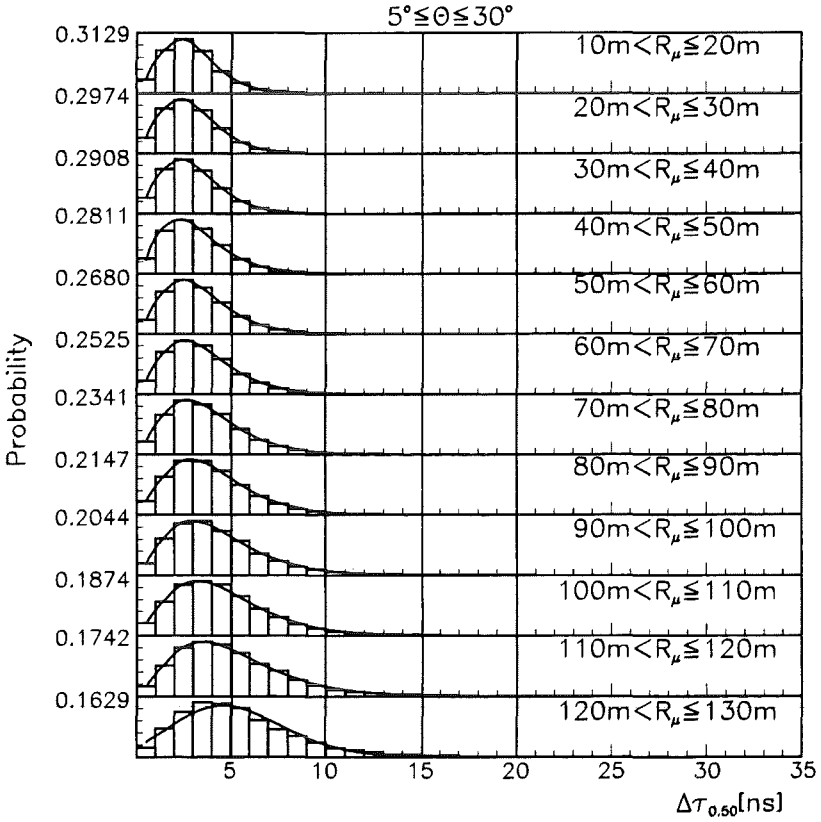

Figure 6: *The variation of the shape of the median distribution (studied up to* $\Delta\tau_{0.5} \leq 75$ *ns) with the core distance, corresponding to the* N_μ^{tr} *spectrum of the observed sample and for* $5^o \leq \theta \leq 30^o$. *The distributions are normalised to the maximum number of particle per time-bin. The lines give the fits by the* Γ- *form.*

The Γ-form proves to be empirically justified and convenient form that fits well the bulk of the experimental data. In Figures 6-8 the Γ-form has been applied to the muon component and show that the overall distributions can be well represented, only in the case of $\Delta\tau_{0.75}$ the longer tails of the distributions are less well described.

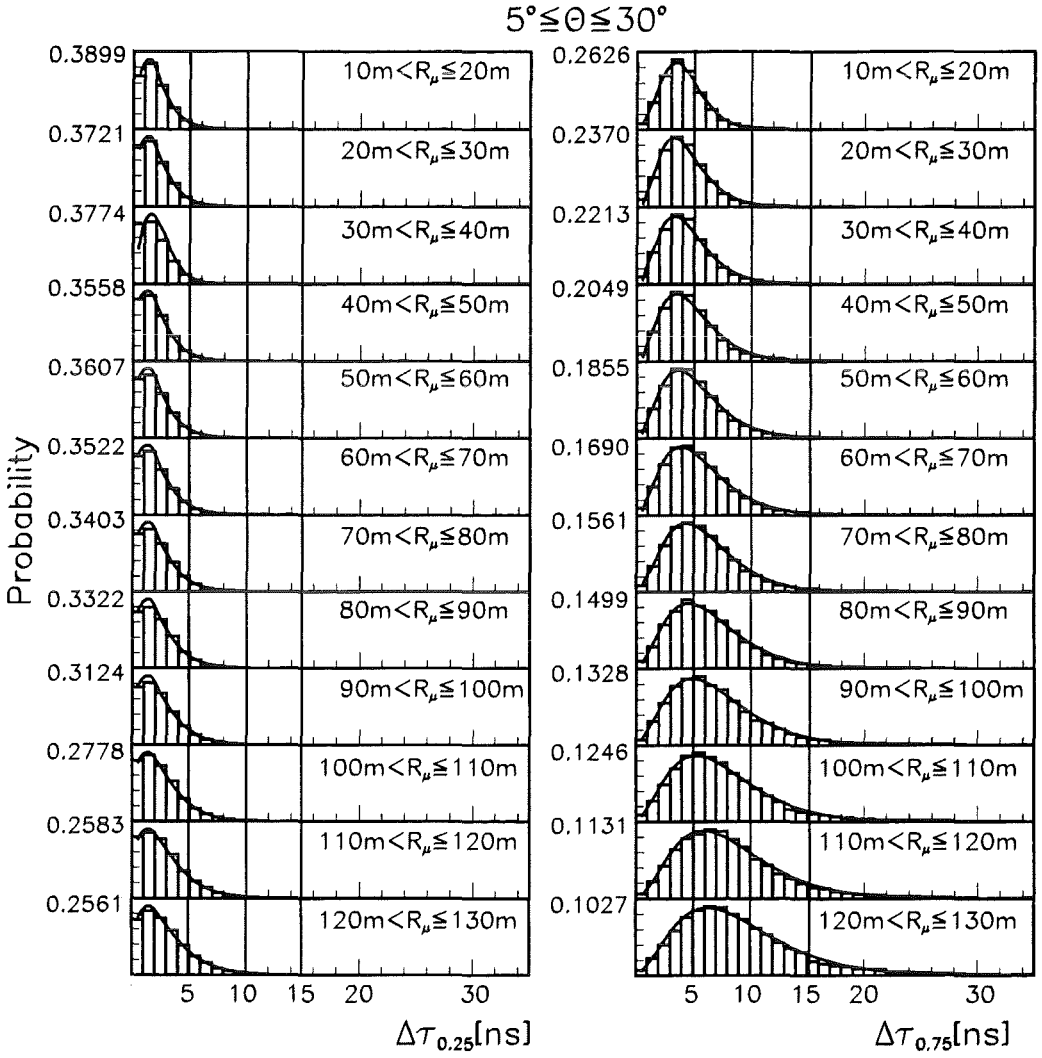

Figure 7: *The variation of the shape of the distributions of the* 1^{st} *and* 3^{rd} *quartiles with the core distance, averaged over the* N_μ^{tr} *spectrum of the observed sample and for* $5^o \leq \theta \leq 30^o$. *The distributions are normalised to the maximum number of particle per time-bin. The lines give the fits by the* Γ- *form.*

In Fig. 9 the average median time profile for different zenith angle bins is shown. As obvious, in the angular range up to 30^o (where secθ varies from 1.0 to 1.15) the angular dependence is practically negligible, but it is not insignificant for larger zenith angles. The shape of the EAS muon time profiles ($< \Delta\tau >, \sigma$; $< \Delta\tau_{0.5} >, \sigma_{0.5}$; $< \Delta\tau_{0.25} >, \sigma_{0.25}$; $< \Delta\tau_{0.75} >, \sigma_{0.75}$) may be approximated by a parabolic form

$$T(R_\mu) \;=\; t_1 + t_2(R_\mu/R_m)^\beta \qquad (4.2)$$

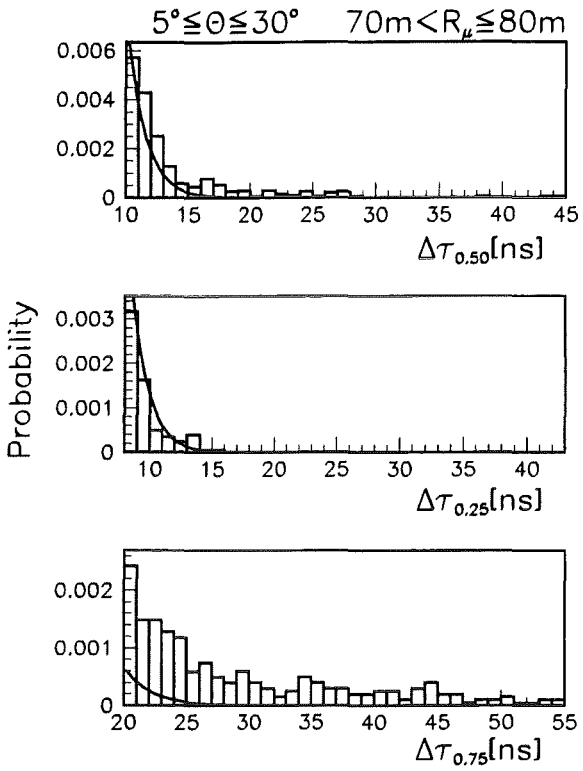

Figure 8: *Tails of the distributions of the median, first and third quartiles as compared with the fits by the Γ-form.*

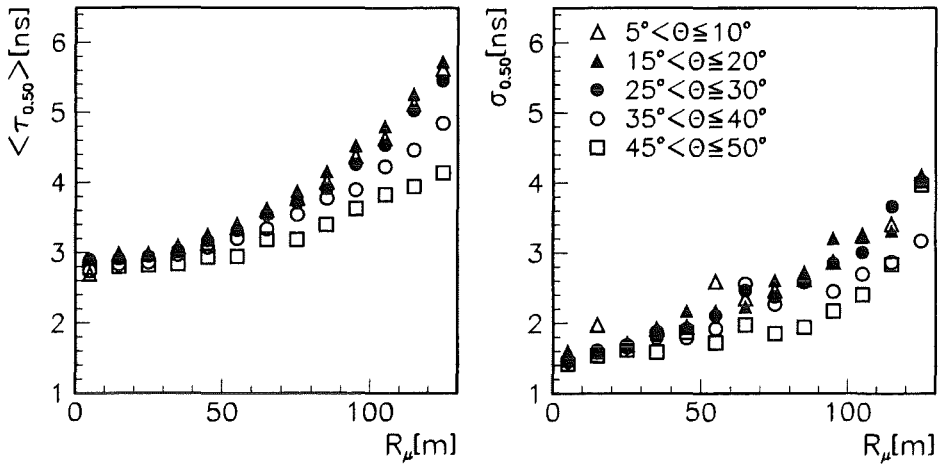

Figure 9: *Average median time profiles* ($< \Delta\tau_{0.5} >, \sigma_{0.5}$) *for different bins of the zenith angle* θ *averaged over the* N_e *spectrum* ($\log_{10} N_e < 6.5$).

with R_m the scaling radius for the muon lateral distribution function (determined for $E_\mu \geq 2$ GeV to be $R_m = 100$ m [21]). Due to some deficiencies of the Γ-form in parameterising the long tails there appear systematic differences, in particular in the values of σ and σ^Γ, if the profiles are directly derived from the data histograms or alternatively via the fits to the Γ-form.

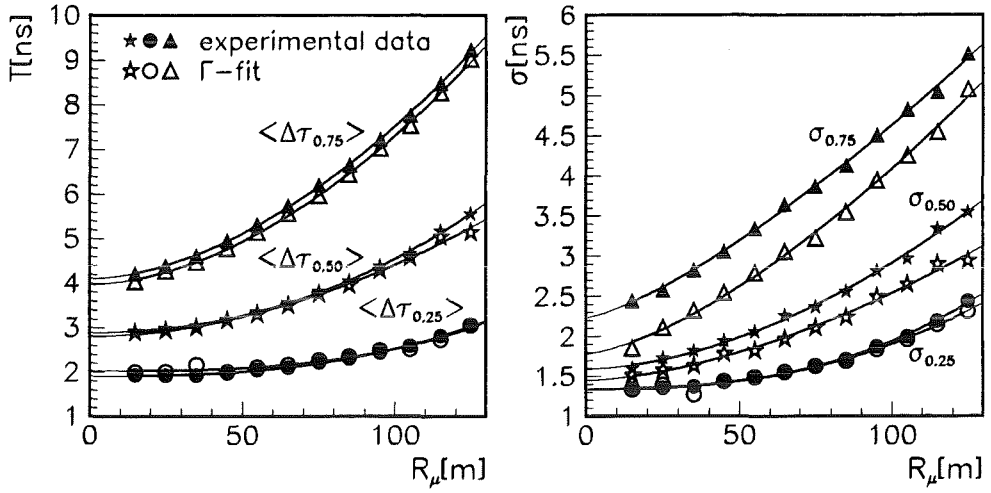

Figure 10: *The mean values and standard deviations of the median, first and third quartiles distributions extracted from the distributions and compared with those from the fitting first the distributions by the* Γ*- form (eq. 4.1).*

In Fig. 10 the results for the mean values and standard deviations extracted directly from the experimental (histograms) distributions are compared with those from fitting first the distributions by the Γ-form (eq. 4.1). It indicates some limitations of the used parameterisation (in particular for the variances). However, the deviations are much smaller than observed for the total charged particle component [3]. We notice the pronounced variation of the third quartile while the first quartile, representing the rise of the "muon pulse" increases more slowly with R_μ. Tab. 1 compiles the results of the parameter adjustments for both procedures. In the following we derive furtheron the profiles directly from the histograms.

$5^o \leq \theta \leq 30^o$

	$< \Delta\tau_{0.25} >$		$< \Delta\tau_{0.5} >$		$< \Delta\tau_{0.75} >$		$< \sigma_{0.25} >$		$< \sigma_{0.5} >$		$< \sigma_{0.75} >$	
	hist.	fit	hist.	fit	hist.	fit	hist.	fit	hist.	fit	hist.	fit
t_1	1.90	1.85	2.90	2.83	4.19	4.14	1.36	1.37	1.77	1.47	2.46	2.13
t_2	0.63	0.61	1.65	1.62	3.52	3.16	0.57	0.55	1.26	1.08	2.79	1.93
β	2.65	2.65	2.17	2.07	1.85	1.95	2.74	2.45	2.11	1.82	1.45	1.82

Table 1: *Parameters of the parabolic time profiles (eq.4.2) of the EAS muon component (data points in 10 m bins in the range of 35 - 125 m), extracted from the histogram and compared to the fitted* Γ*-shapes, averaged over all* N_μ^{tr} *ranges and for* $5^o \leq \theta \leq 30^o$.

4.2 Variation with N_μ^{tr}

In the present analysis we have considered 5 different $\log_{10} N_\mu^{tr}$ ranges, covering an energy range from about $8 \cdot 10^{14}$ to $3.4 \cdot 10^{16} eV$. The Figs. 11, 12 and 13 compare for the angular range of $5^o \leq \theta \leq 30^o$ the distributions of the median values $\Delta\tau_{0.5}$, of the quartiles $\Delta\tau_{0.25}$ and $\Delta\tau_{0.75}$ for two different $\log_{10} N_\mu^{tr}$ ranges.

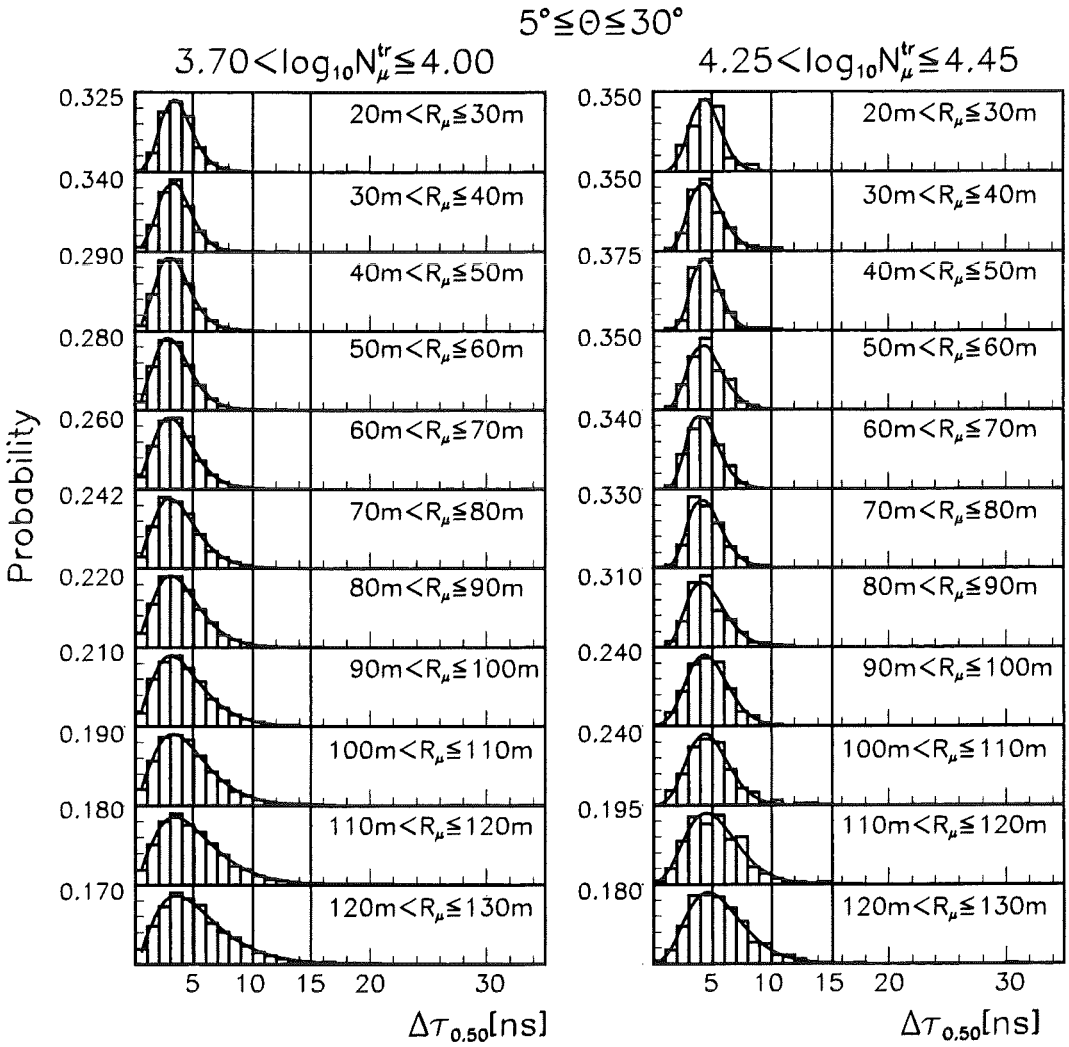

Figure 11: *The variation of the shape of the median distribution with the core distance R_μ for the $\log_{10} N_\mu^{tr}$ ranges 3.70−4.00, 4.25−4.45 and for $5^o \leq \theta \leq 30^o$. The distributions are normalised to the maximum number of particle per time-bin. The lines give the fits by the Γ-form.*

Figure 14 compares profiles for two different $\log_{10} N_\mu^{tr}$ ranges. It shows some peculiarities in the R_μ variation, revealing obvious deviations from a simple monotonic (quasi parabolic) shape of the muon profiles at smaller distances from the EAS centre.

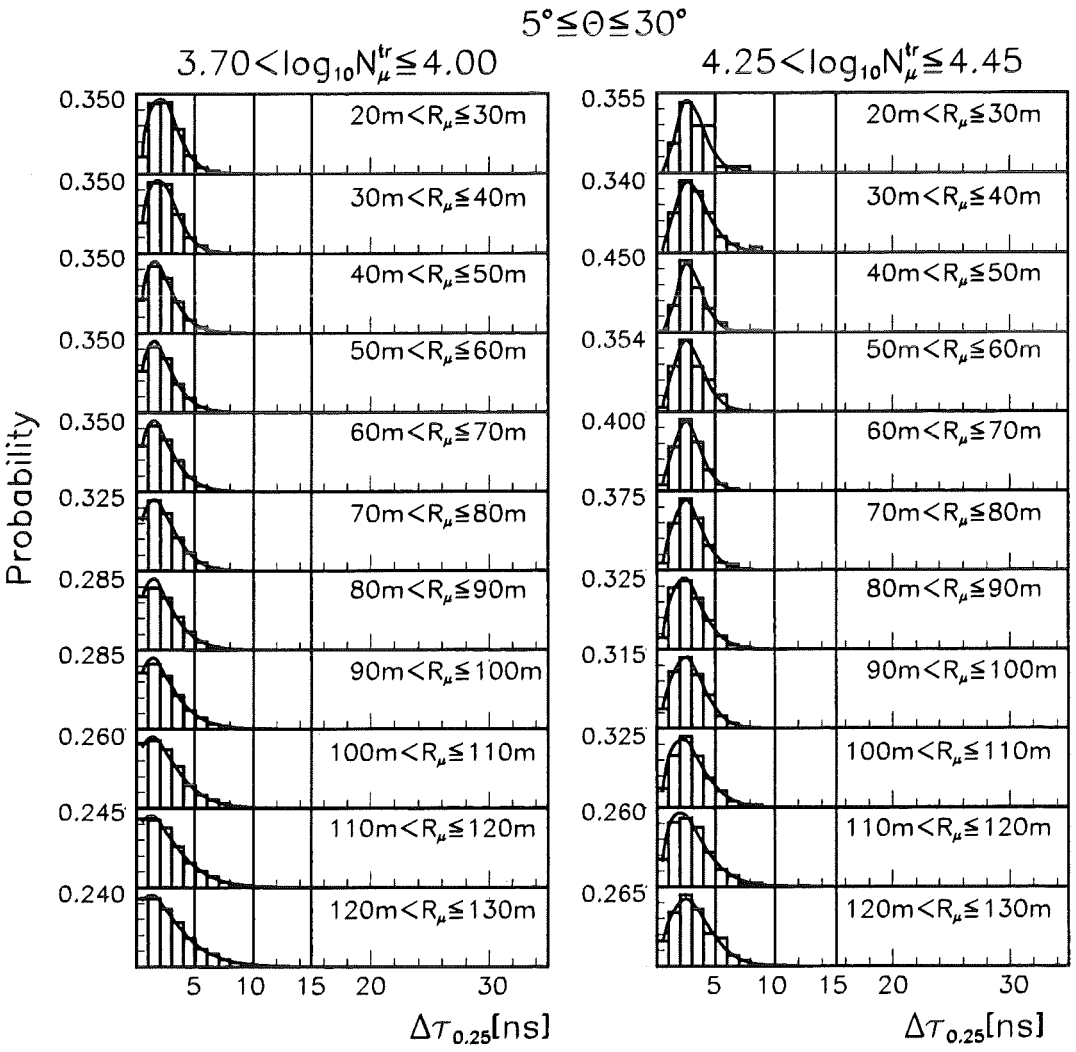

Figure 12: *The variation of the shape of the first quartile distribution with the core distance R_μ for the $\log_{10} N_\mu^{tr}$ ranges $3.70 - 4.00, 4.25 - 4.45$ and for $5^o \leq \theta \leq 30^o$. The distributions are normalised to the maximum number of particle per time-bin. The lines give the fits by the Γ-form.*

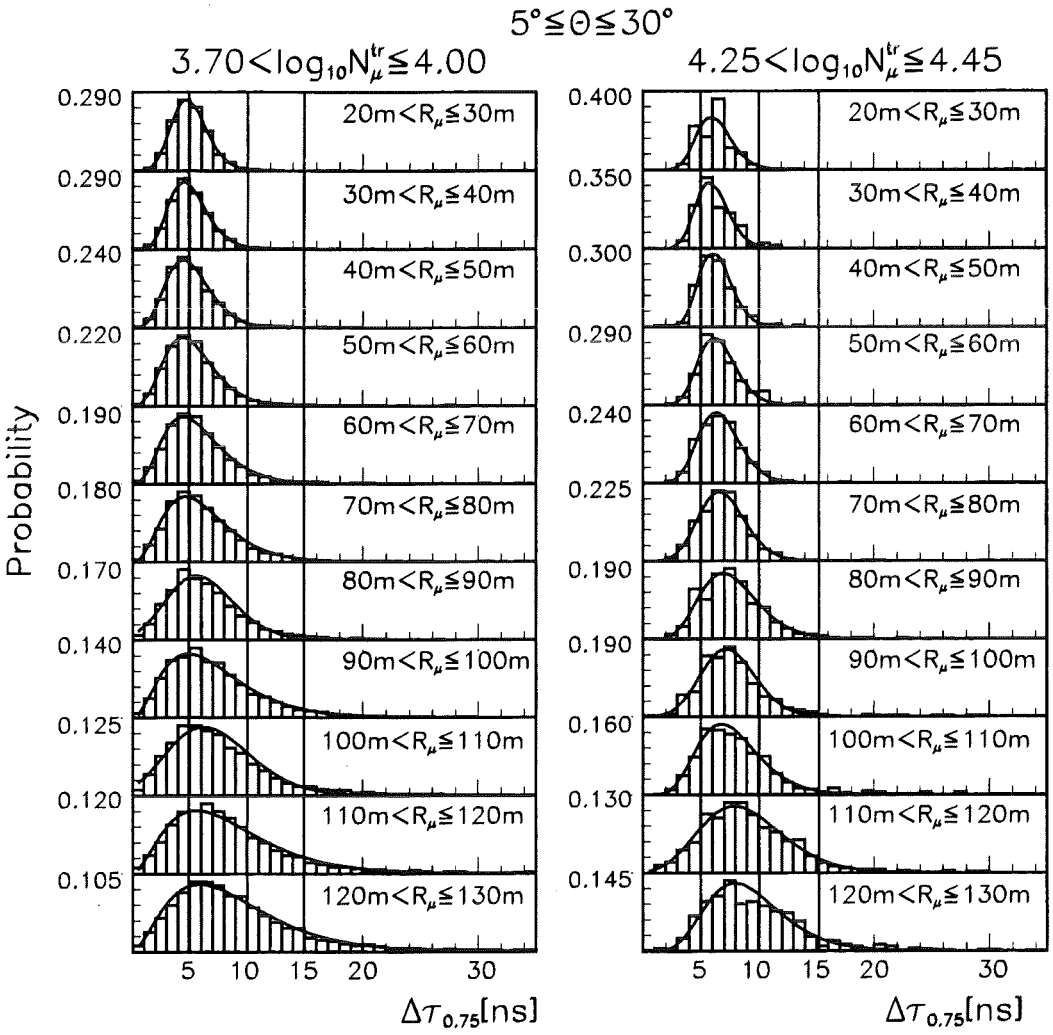

Figure 13: *The variation of the shape of the third quartile distribution with the core distance R_μ for the $\log_{10} N_\mu^{tr}$ ranges $3.70 - 4.00, 4.25 - 4.45$ and for $5^o \leq \theta \leq 30^o$. The distributions are normalised to the maximum number of particle per time-bin. The lines give the fits by the Γ-form.*

The origin of the features indicated in Fig. 14 has been identified to be due to statistical effects in estimating the moments (like the median) of the probability density function (PDF) from small samples of events. The present studies consider time distributions relative to the arrival time of the foremost muon and with muon multiplicities $n \geq 3$. Following the considerations of ref. [22] it can be shown that the arrival time T_μ^1 of the foremost muon (relative to a fictive time - zero, representing the muon front and approximated with a sample of very large n), its fluctuations and the estimated median value e.g. of $\Delta\tau^{loc} = T_\mu - T_\mu^1$ depend on the particular value of the multiplicity n, systematically increasing the mean values of the moments with increasing n. The actual observed profiles (Fig. 14) are derived from samples $T_\mu^1, T_\mu^2 ... T_\mu^n$ of *different* muon multiplicities, with the average multiplicities depending on R_μ and increasing with the core distance, for the case of different $\log_{10} N_\mu^{tr}$ values differently, according to the lateral muon density distributions. Using a model PDF for the time distributions the observed features can be reproduced by simulation calculations. In addition in the experiment we observe samples composed of EAS events of *different* primaries, which exhibit different lateral muon densities and different arrival time distributions. This would imply that the particular mixture of contributions of different EAS primaries to the observed arrival time distributions is also varying with R_μ. However, as simulation studies show this effect is rather small and inadequate for an efficient mass discrimination.

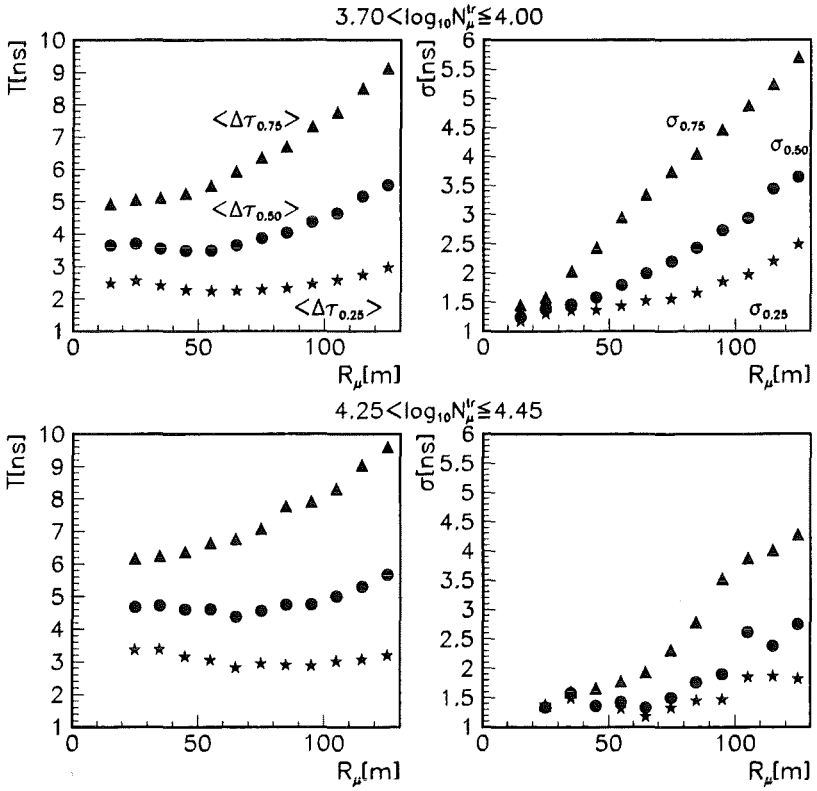

Figure 14: *The mean values and standard deviations of the median, first and third quartiles extracted from the distributions for two different* $\log_{10} N_\mu^{tr}$ *ranges.*

For displaying the gross features of the profiles, excluding the central region of the EAS, fits by eq. 4.2 are given in Figs. 15 and 16 which show the profiles for two different ranges of the zenith angle θ, with a specification of five different $\log_{10} N_\mu^{tr}$ ranges. There is a clear dependence of the profiles on $\log_{10} N_\mu^{tr}$, expressed by the parameters compiled in Table 2.

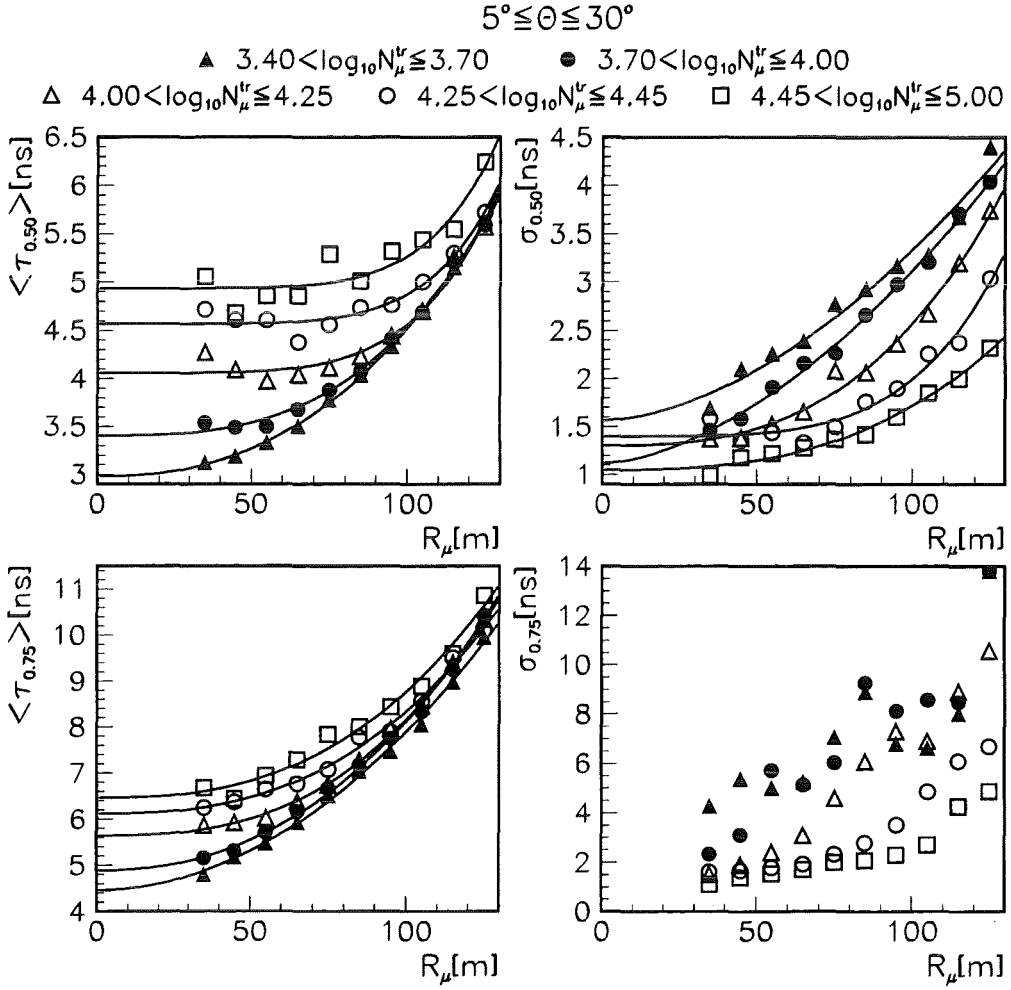

Figure 15: *The R_μ dependence of the mean values and of the standard deviations of the median, first quartile and third quartile distributions for different ranges of* $\log_{10} N_\mu^{tr}$ *in the zenith-angle range of* $5^o \leq \theta \leq 30^o$. *Full lines are approximations of the time profile by a parabolic shape.*

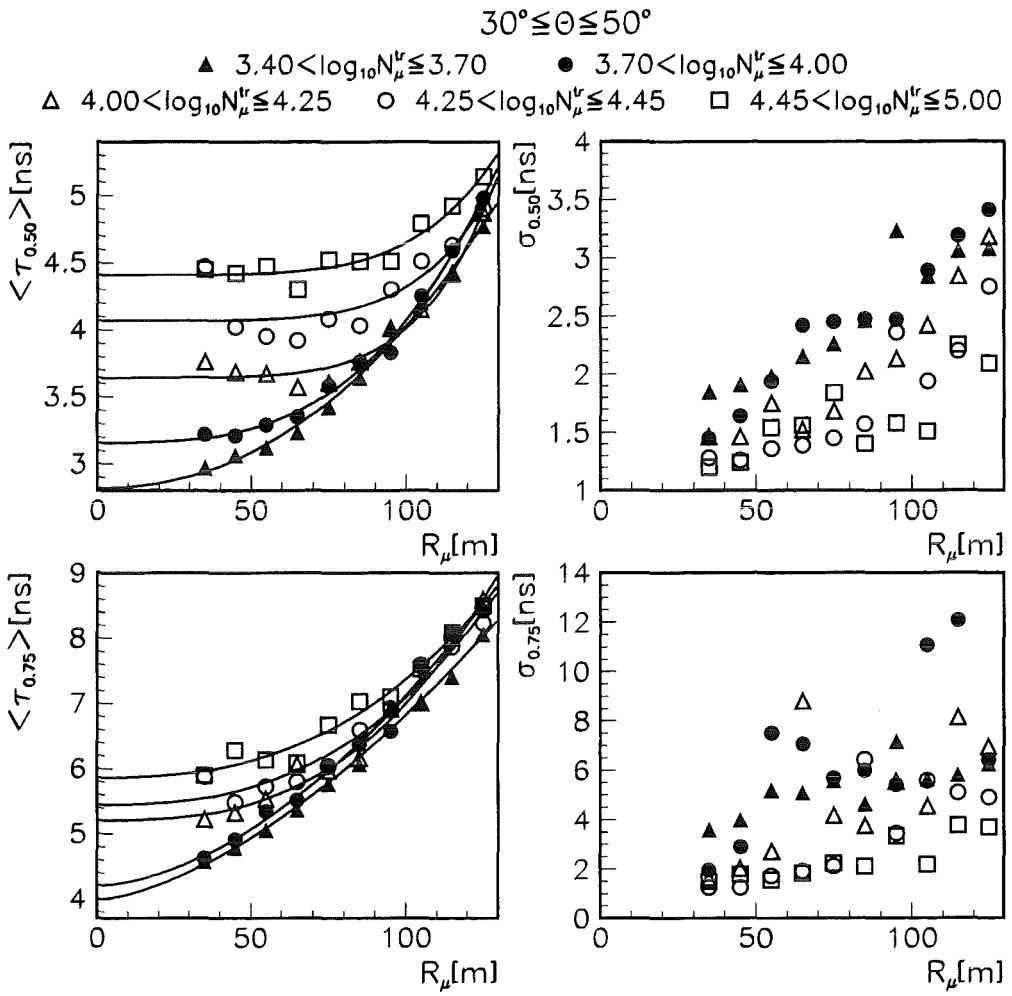

Figure 16: *Time profiles: The R_μ dependence of the mean values and of the standard deviations of the median, first quartile - and third quartile distributions for different ranges of* $\log_{10} N_\mu^{tr}$ *in the zenith-angle range of* $30^o \leq \theta \leq 50^o$. *Full lines are approximations of the time profile by a parabolic shape.*

In appendix B the variation of the mean moments and their dispersions with $\log_{10} N_\mu^{tr}$ is specified for some particular larger ranges of R_μ and of the zenith angle θ.
It is obvious that the standard deviations of the distributions generally decrease with increasing primary energy E_0 ($\log_{10} E_0 \propto \log_{10} N_\mu^{tr}$), and that this is particularly pronounced for the third quartile, indicating the larger fluctuations of the tails of the delayed arrival time distributions. Actually such seemingly irregular fluctuations of $\sigma_{0.75}$ are reproduced by EAS simulations. The dependence on the zenith-angle will be detailed in context of a consideration of fluctuations of the height of EAS maximum (sect. 5).

$5^o < \theta \leq 30^o$	t_1				
$\log_{10} N_\mu^{tr}$	$< \Delta\tau_{0.25} >$	$< \Delta\tau_{0.5} >$	$< \Delta\tau_{0.75} >$	$< \sigma_{0.25} >$	$< \sigma_{0.5} >$
3.40-3.70	1.95	1.31	2.97	1.58	4.46
3.70-4.00	2.27	1.33	3.40	1.13	4.88
4.00-4.25	1.37	1.31	4.06	1.31	5.65
4.25-4.45	1.49	1.32	4.57	1.40	6.12
4.45-5.00	1.71	0.80	4.90	1.05	6.45
$5^o < \theta \leq 30^o$	t_2				
$\log_{10} N_\mu^{tr}$	$< \Delta\tau_{0.25} >$	$< \Delta\tau_{0.5} >$	$< \Delta\tau_{0.75} >$	$< \sigma_{0.25} >$	$< \sigma_{0.5} >$
3.40-3.70	0.49	0.70	1.55	1.76	3.44
3.70-4.00	0.22	0.57	1.13	2.00	3.25
4.00-4.25	1.37	0.41	0.51	1.27	2.52
4.25-4.45	1.49	0.22	0.30	0.60	2.22
4.45-5.00	1.71	0.66	0.43	0.67	2.33
$5^o < \theta \leq 30^o$	β				
$\log_{10} N_\mu^{tr}$	$< \Delta\tau_{0.25} >$	$< \Delta\tau_{0.5} >$	$< \Delta\tau_{0.75} >$	$< \sigma_{0.25} >$	$< \sigma_{0.5} >$
3.40-3.70	3.34	2.59	2.41	1.77	2.00
3.70-4.00	5.31	3.11	3.06	1.70	2.29
4.00-4.25	0.01	4.15	5.12	2.86	2.79
4.25-4.45	-0.12	4.26	6.13	4.41	2.66
4.45-5.00	-0.01	0.84	4.83	2.78	2.63
$30^o < \theta \leq 50^o$	t_1				
$\log_{10} N_\mu^{tr}$	$< \Delta\tau_{0.25} >$	$< \Delta\tau_{0.5} >$	$< \Delta\tau_{0.75} >$	$< \sigma_{0.25} >$	$< \sigma_{0.5} >$
3.40-3.70	1.81	1.26	2.82	1.22	3.98
3.70-4.00	2.06	1.29	3.16	0.45	4.20
4.00-4.25	1.23	1.33	3.64	1.44	5.20
4.25-4.45	1.36	1.09	4.07	1.19	5.44
4.45-5.00	1.50	0.76	4.41	0.97	5.86
$30^o < \theta \leq 50^o$	t_2				
$\log_{10} N_\mu^{tr}$	$< \Delta\tau_{0.25} >$	$< \Delta\tau_{0.5} >$	$< \Delta\tau_{0.75} >$	$< \sigma_{0.25} >$	$< \sigma_{0.5} >$
3.40-3.70	0.42	0.51	1.21	1.58	2.84
3.70-4.00	0.21	0.45	0.91	2.39	2.91
4.00-4.25	1.23	0.34	0.37	0.84	1.79
4.25-4.45	1.36	0.58	0.25	0.80	1.65
4.45-5.00	1.50	0.76	0.24	0.83	1.51
$30^o < \theta \leq 50^o$	β				
$\log_{10} N_\mu^{tr}$	$< \Delta\tau_{0.25} >$	$< \Delta\tau_{0.5} >$	$< \Delta\tau_{0.75} >$	$< \sigma_{0.25} >$	$< \sigma_{0.5} >$
3.40-3.70	2.45	2.06	2.17	1.04	1.58
3.70-4.00	5.28	2.74	3.13	0.80	1.76
4.00-4.25	0.08	4.06	5.43	3.31	2.84
4.25-4.45	-0.06	1.79	5.59	2.74	2.62
4.45-5.00	-0.11	0.55	5.07	1.09	2.56

Table 2: *Parameters of the parabolic time profiles of the EAS muon component (data points in 10 m bins in the range of 45 - 125 m) extracted directly from the experimental data for different ranges of* $\log_{10} N_\mu^{tr}$ *and of the zenith-angle of shower incidence.*

From the present analysis of the phenomenological features of temporal structure of the muon component ($E_\mu \geq 2$ GeV) we conclude:

- The EAS muon disc can be characterised by the R_μ dependence of various different moments $\Delta\tau, \Delta\tau_{0.5}, \Delta\tau_{0.25}, \Delta\tau_{0.75}$.

- The general shape of these distributions can be well parameterised by the Γ-probability distribution function.

- In a wide range, not too close to the shower core the time profiles represented by the mean and dispersion of these moment distributions ($< \Delta\tau >$, σ; $< \Delta\tau_{0.5} >$, $\sigma_{0.5}$; $< \Delta\tau_{0.25} >$, $\sigma_{0.25}$; $< \Delta\tau_{0.75} >$, $\sigma_{0.75}$) can be approximated by a parabolic shape in a R_μ range up to 130 m. There are some features which deviate from a monotonic behaviour, when studying the dependence on different $\log_{10} N_\mu^{tr}$ sizes. These are understood as effects arising from the superposition of time distributions of varying muon multiplicities of relatively small numbers n, with systematic effects in estimating the moments.
  The fast component represented by the first quartile shows a slow increase with R_μ as compared to the third quartile.

- The EAS profiles for muons prove to be significantly flatter than for the charge particle component.

- Though the variations with the energy and zenith angle appear to be not very pronounced at a first glance, for larger zenith angles they are significant and encouraging for an analysis in terms of the elongation rate and fluctuations of the shower maximum.

5 Information on elongation rate and fluctuations of the shower maximum

The average depth of the maximum X_m of the shower development depends on the energy E_0 and the mass of the primary particle, and its dependence on the energy is traditionally expressed by the so-called elongation rate D_e [23], defined as change in the average depth of the maximum per decade of E_0:

$$D_e = dX_m/d\log_{10} E_0 \tag{5.1}$$

Taking into account the (smooth) energy dependence of the multiplicity production and of the hadronic cross sections, reducing D_e from the radiation length X_0 in air by a parameter B, the elongation rate is usually written

$$D_e = (1 - B)X_0 \tag{5.2}$$

Invoking the superposition model approximation that a heavy primary (A) has the same shower elongation rate like a proton, but scaled with energies E_0/A

$$X_m = X_1 + (1 - B)X_0 \log_{10}(E_0/A) \tag{5.3}$$

or for a mixed composition, characterised by $< \log_{10} A >$

$$< X_m >= X_1 + (1 - B)X_0(\log_{10} E_0 - < \log_{10} A >) \tag{5.4}$$

As long as B is only weakly dependent on the energy, X_m shows practically a linear dependence on $\log_{10} E_0$, and any change in this dependence is indicative for a change either of B or of the composition ($< \log_{10} A >$). Monte Carlo simulation studies of the EAS longitudinal development suggest a value of $D_e = (80 \pm 11)\text{gcm}^{-2}$ per decade [24] while experimental investigations tend, though with large spread, to smaller values (see ref. [8], [23]). The HEGRA collaboration has recently communicated as preliminary result $D_e = (52 \pm 2 \pm 10)\text{gcm}^{-2}$ per decade [25].
An indirect approach studying D_e has been suggested by Linsley in 1977 [23] and can be applied to shower parameters which do not depend explicitly on the energy of the primary particle, but do depend on the depth of observation X and on the depth X_m of shower maximum. The quantities (the arrival times and their dispersions) characterising the time structure of the muon shower disc and reflecting the longitudinal EAS development, are of this type and have been scrutinised under this aspect by Walker and Watson in 1981 [8] and by Blake et al. [7].
Following the notation given there we write for the time quantities like $T = f(X, X_m)$

$$\partial T/\partial \log_{10} E_0 \mid_X = D_e \partial T/\partial X_m \mid_{E_0} \tag{5.5}$$

The change of T with the energy E_0 at a given observation level $X = X_v/cos\theta$ (with vertical atmospheric thickness $X_v = 1020\text{gcm}^{-2}$ for the KASCADE level) is proportional to the variation of T with X_m for a given energy. However, at observation level we do not observe $\partial T/\partial X_m$, but $\partial T/\partial X$, which could be related if specifying the function $f(X, X_m)$ and

$$F = -(\partial f/\partial X_m)/(\partial f/\partial X) \tag{5.6}$$

respectively. Thus

$$\partial T/\partial \log_{10} E_0 \mid_X = -FD_e \cdot 1/X_v \cdot \partial T/\partial \sec\theta \mid_{E_0} \tag{5.7}$$

In order to derive from the energy variation of the arrival time quantities information about elongation rate, some knowledge is required about F in addition to the variation with the depth of observation and the zenith-angle dependence, respectively.
In ref. [8] two extreme forms of $f(X, X_m) = f(X - X_m)$ or $f(X, X_m) = f(X/X_m)$ are scrutinised with $F = 1$ or $F = X/X_m$, respectively have been scrutinised on the basis of experimental data, favouring the case $F = 1$.
In a similar way the fluctuations $\sigma(X_m)$ of X_m, which indicate the mass composition of

primary cosmic rays [9], can be related to the fluctuations $\sigma(T)$ of T by

$$\sigma(X_m) = -\sigma(T) \cdot X_v/(\partial T/\partial \sec\theta) \mid_{E_0} \tag{5.8}$$

For evaluating the above relations the variation of the measured time quantities with the angle of shower incidence and with N_μ^{tr} has to be considered, i.e. $\epsilon_E = \partial T/\partial \log_{10} N_\mu^{tr} \mid_{\sec\theta}$ and $\epsilon_\theta = \partial T/\partial \sec\theta \mid_{N_\mu^{tr}}$ must be extracted from the data. Following the results of simulation studies the relation: $\log_{10} E_0[GeV] = 2.28 + 1.04 \cdot \log_{10} N_\mu^{tr}$ is adopted.
Just for a first impression Fig. 17 displays the dependence of the time moments T $(< \Delta\tau >, < \Delta\tau_{0.5} >, < \Delta\tau_{0.25} >, < \Delta\tau_{0.75} >)$ *from* $\sec\theta$ *for different regions of* R_μ*, averaged over the observed* N_μ^{tr} *range. In appendix B these dependences are further specified for different* $\log_{10} N_\mu^{tr}$ *ranges. Neglecting an atmospheric pressure dependence, the variation with* $\sec\theta$*, being understood as the X- dependence is linearly approximated by* $T = z_0 + \partial T/\partial \sec\theta \cdot \sec\theta$*. The parameters* z_0 *and* $\partial T/\partial \sec\theta$ *are given in Table 3 of the appendix B for all time quantities* T $(< \Delta\tau >, < \Delta\tau_{0.5} >, < \Delta\tau_{0.25} >, < \Delta\tau_{0.75} >)$*. The obtained results are consistent with observations of Walker and Watson [8] at larger distances from the shower core. In Ref. [26] on basis of geometrical considerations it had been argued (and shown for a data sample averaged on the observed shower size spectrum) that* $\partial T/\partial \sec\theta$ *follows a quadratic dependence from* R_μ*.*

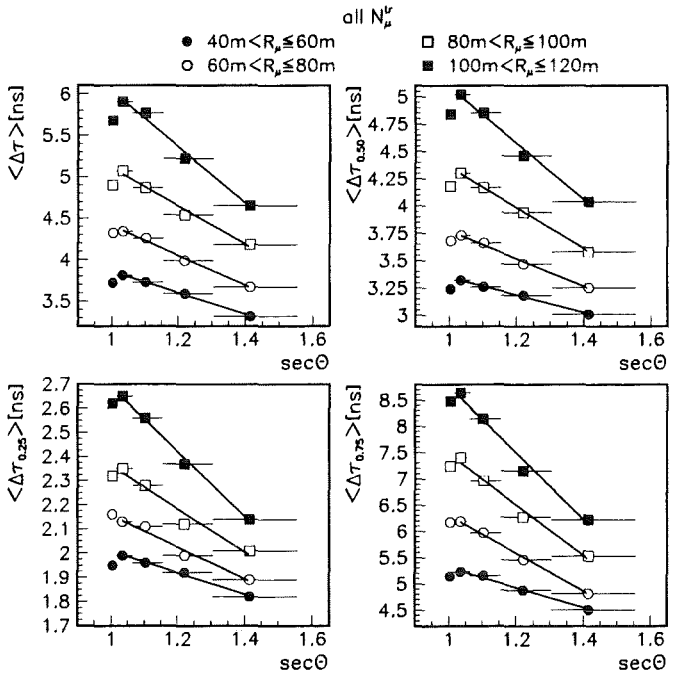

Figure 17: *The variation of* T $(< \Delta\tau >, < \Delta\tau_{0.5} >, < \Delta\tau_{0.25} >, < \Delta\tau_{0.75} >)$ *with the zenith angle* $(\sec\theta)$ *for different radial distances* R_μ*, averaged on the* $\log_{10} N_\mu^{tr}$ *range (3.7- 5.0).*

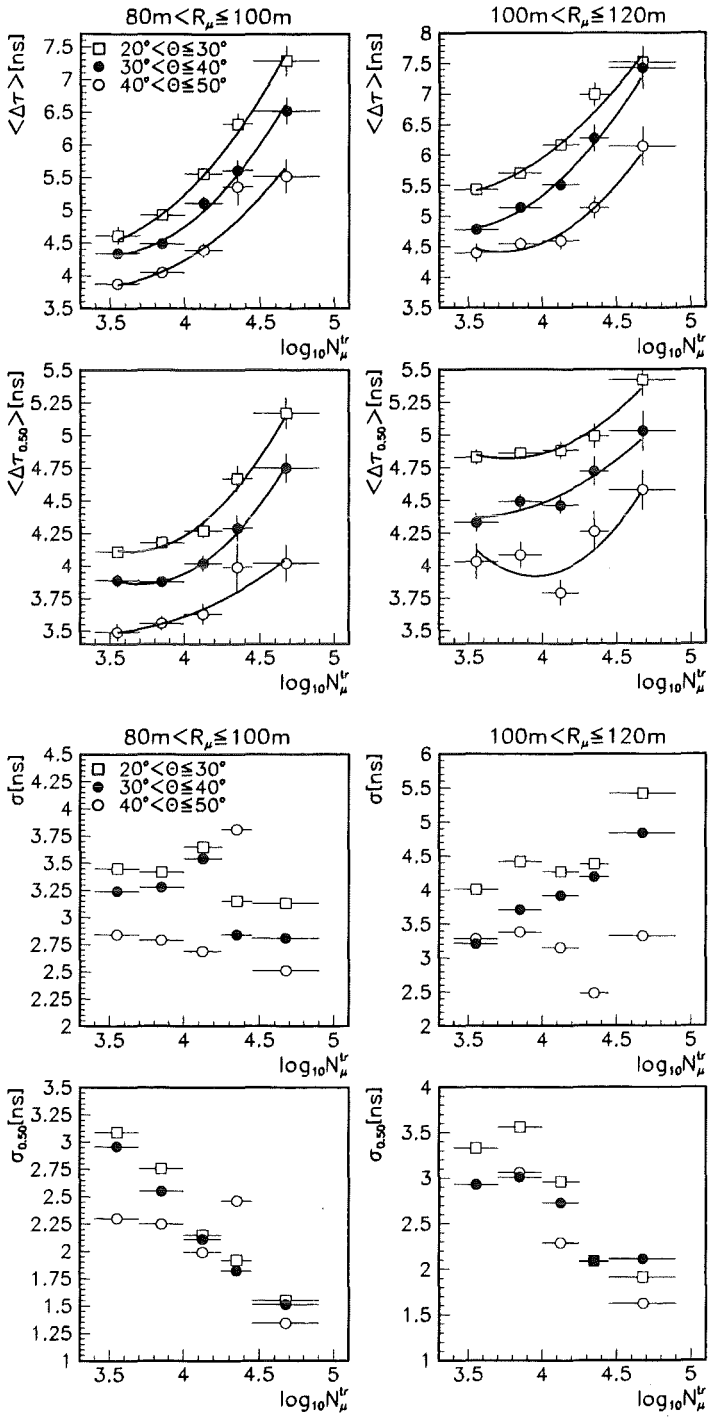

Figure 18: *The variation of the mean value* $< \Delta\tau_{0.5} >$ *of the median distributions and of* $\sigma_{0.5}$*, with* $\log_{10} N_\mu^{tr}$ *for two different distances of the shower core and different ranges of the angle of the EAS coincidence.*

Figure 18 displays the variation with $\log_{10} N_\mu^{tr}$. In order to derive ϵ_E, the $\log_{10} N_\mu^{tr}$ variation has been described by a quadratic form.
Figures 17 and 18 indicate also the hampered accuracy of the results on the variations which is due to the limited actual data base. It appears too premature to evaluate the present data with respect to values of D_e and of the fluctuations of X_m, since the quantities ϵ_E and ϵ_θ are sensitively affected by data inaccuracies. In addition, a serious analysis has to invoke a simulation of the influence of the detector response. This is particularly true for the fluctuations as the real (EAS genuine) fluctuations may be quite smaller than the measured ones. This feature has been indicated in Ref. [27] by studies on basis of Monte Carlo simulations of muon arrival time distributions. Taking into account a rough estimate of the correction, we would result, e.g. in values of D_e and $\sigma(X_m)$ of about 100 g cm^{-2} or less, which is in the expected order of magnitude. In addition, though with large statistical uncertainties (we will not specify quantitatively), we may tentatively infer a tendency indicating some irregular changes of the parameters in the range of $\log_{10} N_\mu^{tr} > 4.0$. In case that such tendencies could be confirmed with a larger statistical accuracy, using a data set allowing a binning in smaller $\log_{10} N_\mu^{tr}$ ranges of the data samples, such an observation would be quite interesting.

6 Concluding remarks

"Utere tempore"
Epikur, (341-270 a. Ch. n.)

With the present studies of the time structure of the EAS muon component inferred from data measured with the KASCADE detector the phenomenological features and dependences of the muon arrival time distributions and of the shower profiles (defined as the dependences of various time moments from distance from the shower core) are reported. These results are at disposal for further analyses and interpretations by use of EAS Monte Carlo simulations, exploring the sensitivity to various different hadronic interaction models (used as generators of the MC calculations) or to the mass composition of primary cosmic rays. Invoking an indirect approach [23] which requires to infer from the data the variation of the considered arrival time quantities with the primary energy and the zenith angle of EAS incidence, it has been outlined that such data, if measured with higher statistical accuracy, especially at larger energy, may provide useful information on the elongation rate and the fluctuations of the height of maximum in the longitudinal shower development.

Acknowledgements

We acknowledge the clarifying discussions with A.A. Watson about the information potential of such investigations. We thank Marin Duma for his efficient help in preparing adequate files from the collected data samples for the analysis. The work has been partly

supported by a grant of the Romanian Ministry of Research and Technology as well as by a research grant (No.94964) of the Armenian Government and by the ISTC project A116. The collaborating group of the Cosmic Ray Division of the Soltan Institute of Nuclear Studies in Lodz and of the University of Lodz is supported by the Polish State Committee for Scientific Research (Grant No. 2 P03B 160 12). The KASCADE collaboration work is embedded in the frame of scientific-technical cooperation (WTZ) projects between Germany and Romania (No.RUM-014-97), Armenia (No. 002-98) and Poland (No.92-94).

References

[1] J. Linsley, L. Scarsi and B. Rossi, Phys. Rev. 92 (1961) 485;
J. Linsley and L. Scarsi, Phys. Rev. 128 (1962) 2384

[2] R. Thielert and L. Wiedecke, Z. Phys. 179 (1964) 199

[3] G. Agnetta et al., Astroparticle Physics 6 (1997) 301

[4] M. Ambrosio, C. Aramo, L. Colesariti, T.V. Danilova and A.D. Erlykin, Astroparticle Physics 7 (1997) 329

[5] H. Rebel, G. Völker, M. Föller and A.A. Chilingarian, Journ. Phys. G: Nucl.Part. Phys. 21 (1995) 451;
H. Rebel, in: The Cosmic Ray Mass Composition, Proc. XV Cracow Summer School of Cosmology, 15-19 July, 1996, Lodz, Poland, Uniwersytetu Lodzkiego, 1997, ed. W. Tkaczyk, p. 91

[6] T. V. Danilova, D. Dumora, A. D. Erlykin and J. Procureur, Journ. Phys. G: Nucl. Part. Phys. 20 (1995) 961

[7] P. R. Blake, W. S. Collis, M. Luksys, W. F. Nash and A. J. Sephton, Journ. Phys. G: Nucl. Phys. 16 (1990) 775

[8] R. Walker and A.A. Watson, Journ. Phys. G: Nucl. Phys.7 (1981)1297

[9] H. E. Dixon and K.E. Turver, Proc. Roy. Soc. London A339 (1974) 171

[10] I. M. Brancus, B. Vulpescu, H. Rebel, M. Duma, A.A. Chilingarian, Astroparticle Physics 7 (1997) 343

[11] H. O. Klages et al. - KASCADE Collaboration, Nucl. Phys. (Proc. Suppl.) 52B (1997) 92;
Proc. 25th ICRC (Durban, South Africa) 1997, Vol.8, 297

[12] J. N.Capdevielle et al., KFK-Report 4998, Kernforschungszentrum Karlsruhe (1990);
D. Heck, J. Knapp, J.N. Capdevielle, G. Schatz and T. Thouw, FZKA-Report 6019, Forschungszentrum Karlsruhe (1998)

[13] A. Haungs, J. Kempa, H. Rebel et al. - KASCADE Collaboration, FZKA-Report 6105, Forschungszentrum Karlsruhe (1998)

[14] M. Brendle, U. Raidt, Nucl. Inst. Meth. A412 (1998) 420

[15] W. Hafemann, J. Wentz, A. Haungs, H.-J. Mathes and H. Rebel - KASCADE Collaboration, Verhandlungen der DPG, Frühjahrstagung Freiburg 1998: Teilchenphysik T 402.2

[16] J. H. Weber for the KASCADE Collaboration, 25th ICRC (Durban, South Africa) 1997, Vol. 6, 153

[17] M. Föller U. Raidt for the KASCADE Collaboration, 25th ICRC (Durban, South Africa) 1997, Vol. 6, 149

[18] R. Glasstetter for the KASCADE Collaboration, 25th ICRC (Durban, South Africa) 1997, Vol. 6, 157

[19] C. P. Woidneck and E. Böhm, Journ. Phys A: Math. Gen. 8 (1975) 997

[20] K. V. Bury, Statistical Models in Applied Science (John Wiley, NewYork 1975), p.299

[21] H. Leibrock, FZKA-Report 6098, Forschungszentrum Karlsruhe (1998)

[22] E. J. de Villiers, D. J. van der Walt, P. K. F. Grieder and G. van Urk, Journ. Phys. G: Nucl. Phys. 12 (1986) 547

[23] J. Linsley, 15th ICRC (Plodiv) 1977, Vol. 12, 89

[24] M. D. Rodriguez-Frias, L. del Peral and J. Medina, Astroparticle Physics 8 (1997) 77

[25] A. Lindner, D. Horns, A. Röhring for the HEGRA Collaboration, contribution to the 10th ISVHECRI 1998, Gran Sasso, Italy, July 12-18, 1998

[26] U. Raidt, FZKA-Report 5917, Forschungszentrum Karlsruhe (1997)

[27] I. M. Brancus, B. Vulpescu, H. Rebel, G. Völker, M. Duma, A. A. Chilingarian, FZKA-Report 5835, Forschungszentrum Karlsruhe (1996)

Appendix A Limitations of the shower core distances

Due to the limited lateral extension of the KASCADE array there are natural limitations for a reliable reconstruction of the shower core location at larger distances, and generally for cores located outside the array the accuracy in the EAS specification is decreasing with an increasing fraction of badly reconstructed showers. In the present muon arrival time measurements a multiplicity of at least 3 muons firing the scintillation detectors of the timing facility correlated with a signal in the MWPC is required. For larger core distances this condition selects EAS with larger muon numbers and larger sizes for which the reconstruction problem and the core location may be relieved.

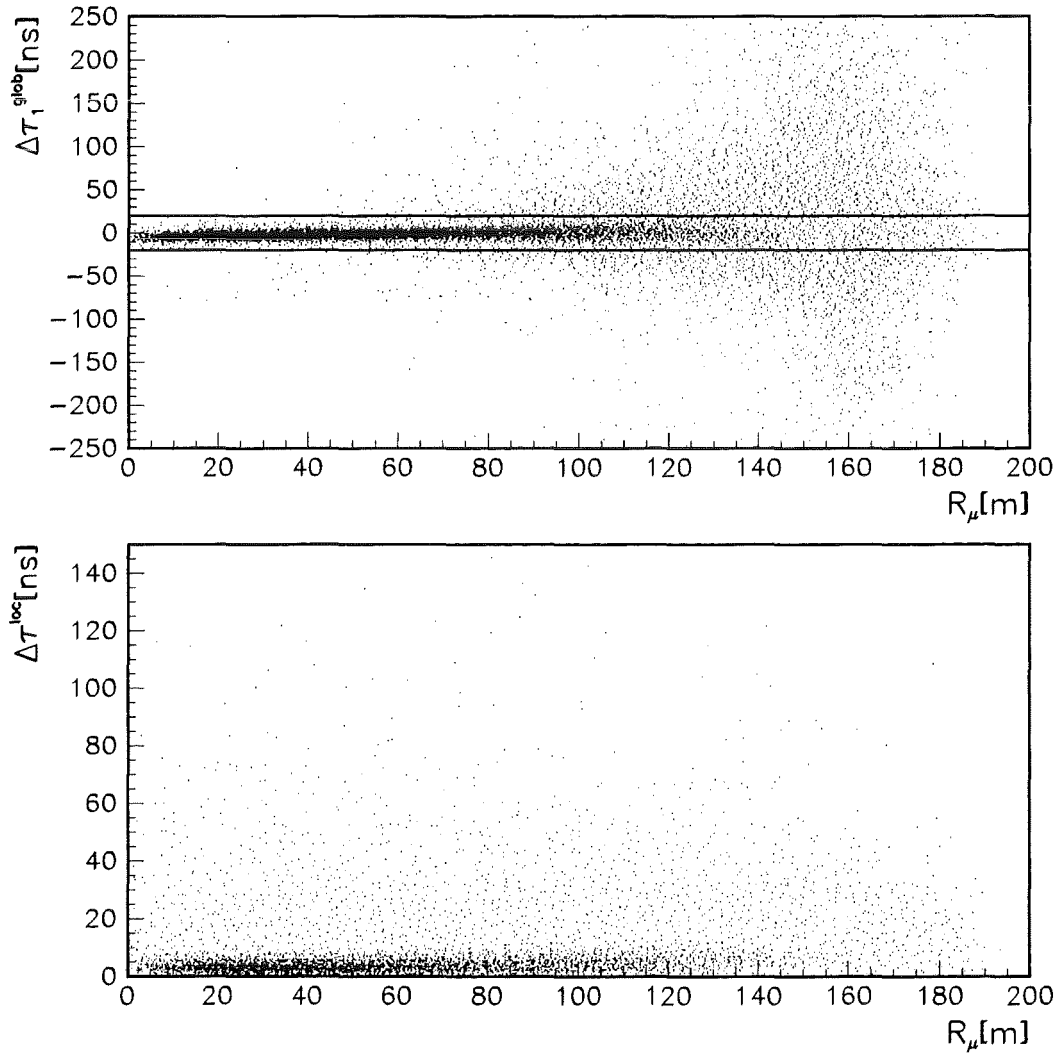

Figure A1: *Distribution of the arrival time of the foremost muon $\Delta\tau_1^{glob}$ relative to the reconstructed arrival time of the shower core and the corresponding distribution of the mean values $\Delta\tau^{loc}$ of the arrival times relative to the foremost muon.*

In order to define the R_μ-range, useful for the determination of the EAS time profiles,

we regarded the global arrival times τ_1^{glob} of the foremost muons (which are in any case affected by some jitter in the reconstruction of the arrival time of the EAS core). As shown in Fig. A1 their values are mostly concentrated in a band of some tens of nanoseconds with only a very small fraction ($< 3 \cdot 10^{-3}$) of events with larger delays τ_1^{glob}. At larger distances with $R_\mu > 100$ m the fraction of these events is increasing, which may be considered as an indication of problems in a correct core reconstruction. Somewhat arbitrarily we limit the maximum R_μ-values to 120 - 130 m when the fraction of events with τ_1^{glob} values outside the indicated band exceeds 0.5 per cent.
To check additionally if there appear any conspicuous anomalies of average shower profiles which may be induced by core location problems for large distances R_μ of the observation, we compared the result for showers which are located in different azimuthal regions of the plane of the KASCADE array. Fig. A2 compares the results for different moments of the local muon arrival time distributions (time profiles) determined for showers located in the diagonal regions ("corners") with those determined for showers located in the direction of half-axis ("middle") of the quadratically arranged detector array. We do not notice any serious warning discrepancy, even not for the 3^{rd} quartile, which is rather sensitive to fluctuations in the tails of the distributions.

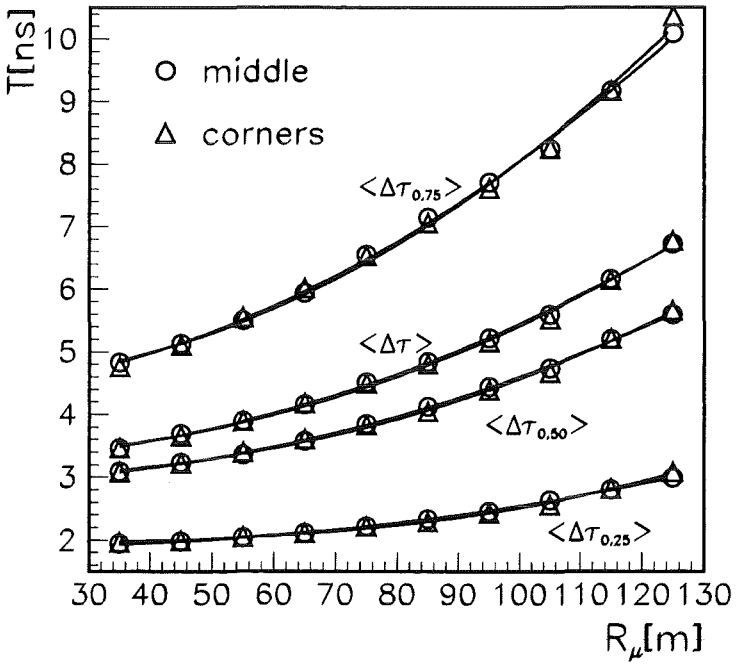

Figure A2: *Comparison of experimental shower profiles determined with showers located in different azimuthal regions of the KASCADE array.*

Thus we conclude that for the present investigation of the average shower profiles the uncertainties of eventual misreconstructions of the location of the core are not noticeable

up to $R_\mu = 120 - 130$ m. Nevertheless this does not exclude that some fluctuations observed in samples of only few showers (e.g. for the EAS with the highest N_μ^{tr} values) might be accidentally affected by the used cuts.
These phenomenologically justified results may be studied and better understood on basis of Monte-Carlo simulations, processed with our current reconstruction and data analysis procedures. Such studies are in progress.

Appendix B The variation of the moments of the muon arrival time distributions with N_μ^{tr} and the zenith angle of shower incidence

In this appendix some results are compiled about the dependence of the EAS time profiles from the energy-indicating EAS observable N_μ^{tr}, particularly specified for different zenith angles of shower incidence and for large R_μ-ranges.

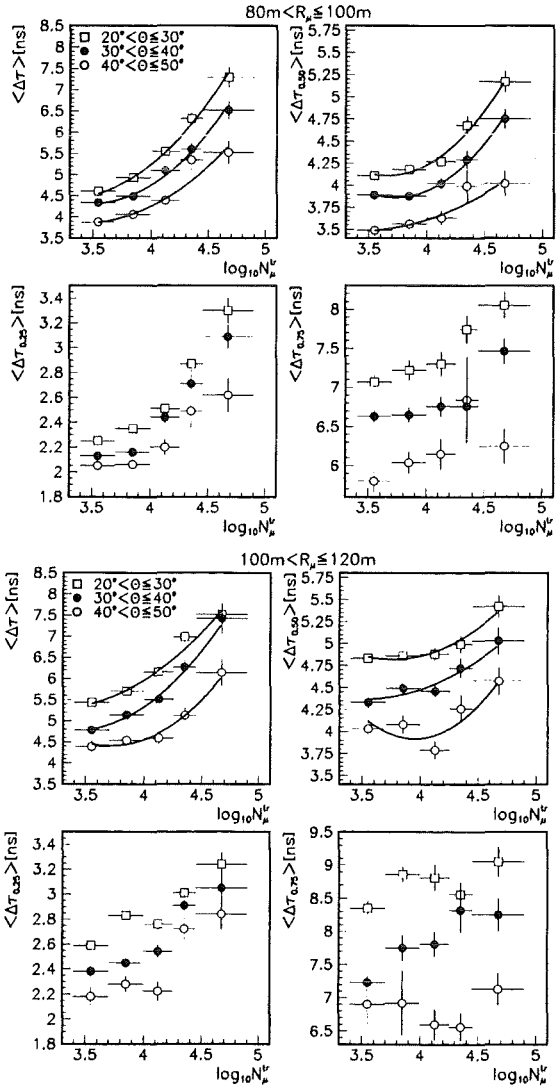

Figure B1: *The variation of the moments* T ($< \Delta\tau >, < \Delta\tau_{0.5} >, < \Delta\tau_{0.25} >, < \Delta\tau_{0.75} >$) *with* N_μ^{tr} *at various zenith angles of shower incidence at large distances* R_μ. *In the case of* $< \Delta\tau >, < \Delta\tau_{0.5} >$ *the dependence has been parameterised by a quadratic form.*

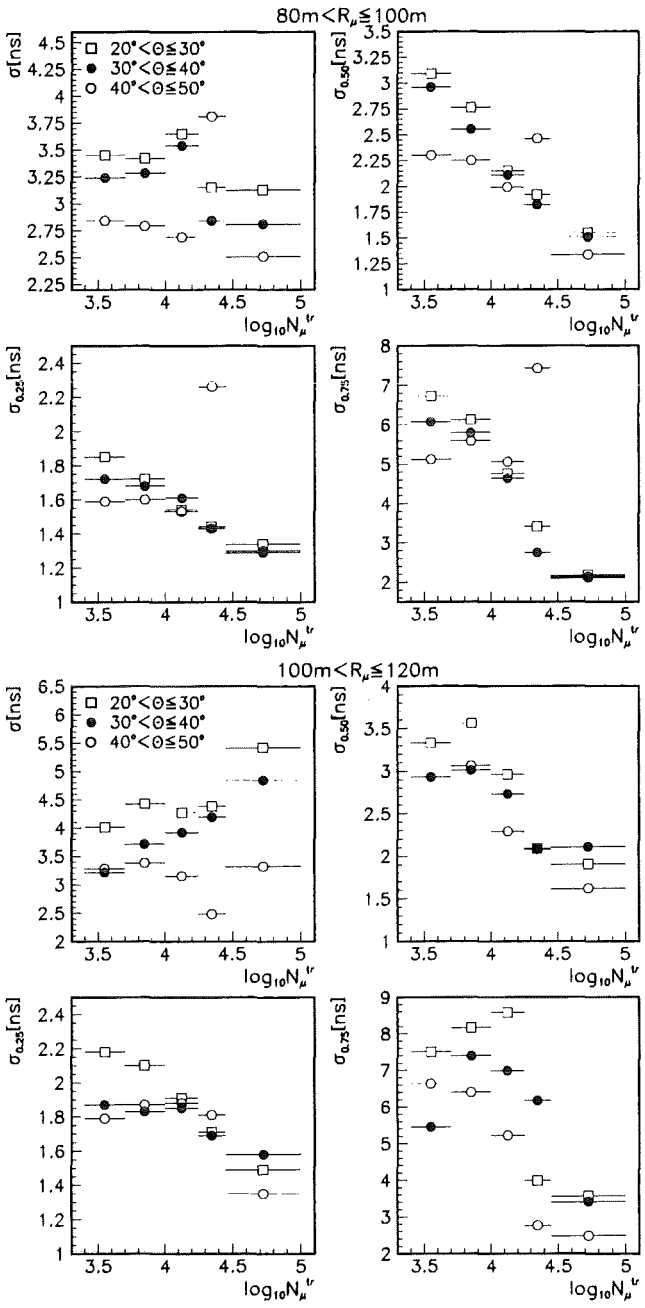

Figure B2: *The variation of the standard deviations* $\sigma, \sigma_{0.5}, \sigma_{0.25}, \sigma_{0.75}$ *with* N_μ^{tr} *at various zenith angles of shower incidence at large distances* R_μ.

Similarly the zenith angle dependence as extracted from the considered data sample, for different ranges of R_μ and specified for different ranges N_μ^{tr}, is shown in Figs. B3 -B4.

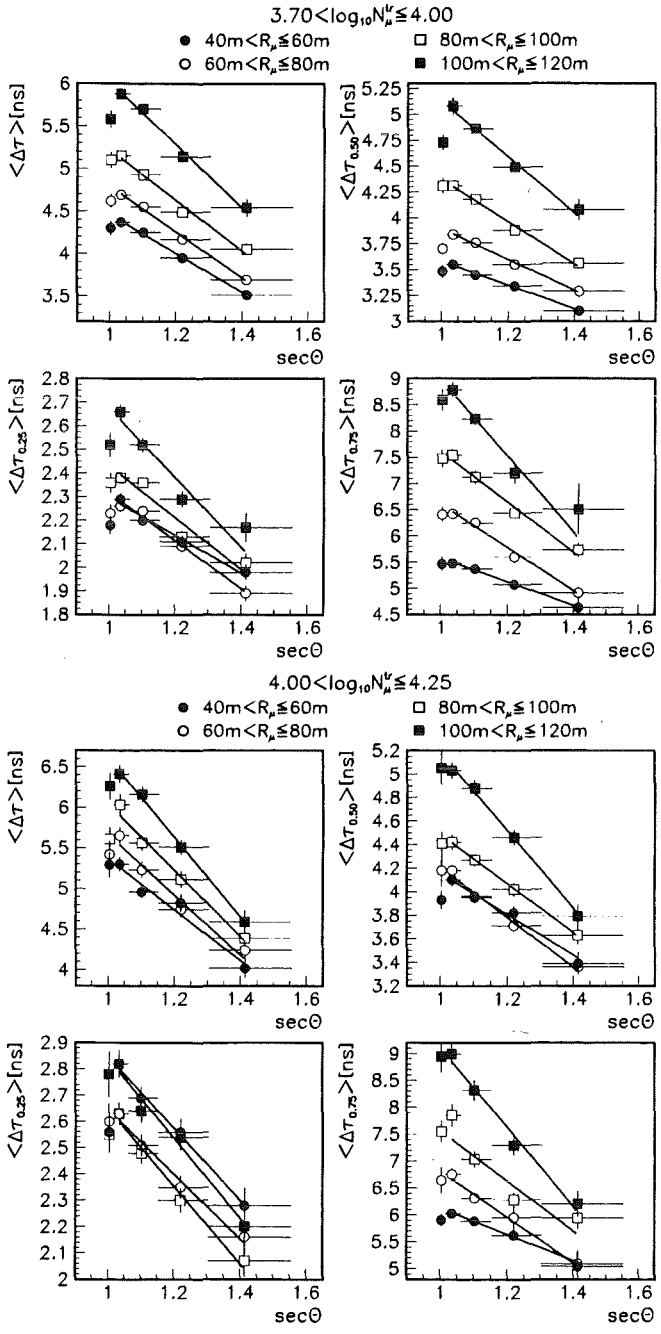

Figure B3: *The variation of T* ($< \Delta\tau >, < \Delta\tau_{0.5} >, < \Delta\tau_{0.25} >, < \Delta\tau_{0.75} >$) *with the zenith angle* (secθ) *for different radial distances* R_μ *and different* $\log_{10} N_\mu^{tr}$ *ranges.*

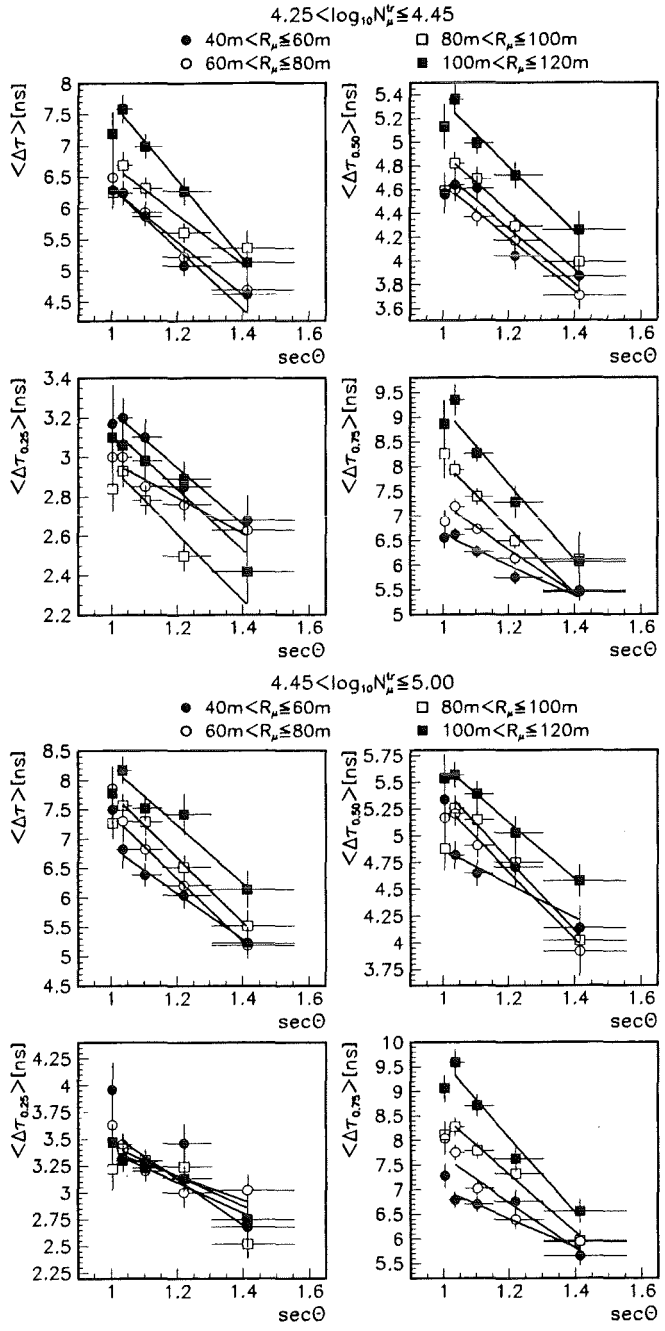

Figure B4: *The variation of* T ($< \Delta\tau >, < \Delta\tau_{0.5} >, < \Delta\tau_{0.25} >, < \Delta\tau_{0.75} >$) *with the zenith angle* ($\sec\theta$) *for different radial distances* R_μ *and different* $\log_{10} N_\mu^{tr}$ *ranges.*

Figures B3 - B4 provide an orientation about the gross features whose details are presently affected by limited statistical accuracy.

$< \Delta\tau >$	z_0[ns]	ϵ_θ	z_0[ns]	ϵ_θ	z_0[ns]	ϵ_θ	z_0[ns]	ϵ_θ	z_0[ns]	ϵ_θ
$\log_{10} N_\mu^{tr}$	3.70 – 4.00		4.00 – 4.25		4.25 – 4.45		4.45 – 5.00		all N_μ^{tr}	
$40 < R_\mu[m] \leq 60$	6.8 ±0.21	-2.3 ±0.18	8.5 ±0.42	-3.2 ±0.37	11.2 ±1.00	-4.9 ±0.87	10.8 ±1.11	-3.9 ±0.93	5.1 ±0.09	-1.3 ±0.08
$60 < R_\mu[m] \leq 80$	7.5 ±0.23	-2.7 ±0.19	9.4 ±0.48	-3.7 ±0.40	10.6 ±0.77	-4.3 ±0.65	12.8 ±1.01	-5.4 ±0.85	6.3 ±0.12	-1.8 ±0.10
$80 < R_\mu[m] \leq 100$	8.2 ±0.25	-3.0 ±0.21	10.1 ±0.45	-4.1 ±0.38	10.7 ±0.98	-4.0 ±0.84	13.3 ±0.97	-5.5 ±0.82	7.5 ±0.15	-2.4 ±0.13
$100 < R_\mu[m] \leq 120$	9.8 ±0.35	-3.7 ±0.30	11.5 ±0.50	-4.9 ±0.42	14.0 ±0.84	-6.3 ±0.69	13.2 ±1.13	-4.9 ±0.98	9.8 ±0.29	-3.7 ±0.24
$< \Delta\tau_{0.50} >$	z_0[ns]	ϵ_θ	z_0[ns]	ϵ_θ	z_0[ns]	ϵ_θ	z_0[ns]	ϵ_θ	z_0[ns]	ϵ_θ
$\log_{10} N_\mu^{tr}$	3.70 – 4.00		4.00 – 4.25		4.25 – 4.45		4.45 – 5.00		all N_μ^{tr}	
$40 < R_\mu[m] \leq 60$	4.7 ±0.15	-1.2 ±0.13	5.9 ±0.30	-1.7 ±0.26	7.1 ±0.50	-2.3 ±0.42	6.5 ±0.70	-1.6 ±0.61	4.1 ±0.07	-0.8 ±0.06
$60 < R_\mu[m] \leq 80$	5.4 ±0.18	-1.5 ±0.16	6.3 ±0.24	-2.1 ±0.20	6.9 ±0.45	-2.2 ±0.39	8.5 ±0.71	-3.2 ±0.62	5.1 ±0.10	-1.3 ±0.08
$80 < R_\mu[m] \leq 100$	6.4 ±0.20	-2.0 ±0.17	6.6 ±0.29	-2.1 ±0.25	7.3 ±0.55	-2.4 ±0.48	8.8 ±0.54	-3.3 ±0.46	6.3 ±0.12	-1.9 ±0.10
$100 < R_\mu[m] \leq 120$	7.8 ±0.36	-2.7 ±0.31	8.5 ±0.35	-3.3 ±0.30	8.1 ±0.56	-2.7 ±0.48	8.3 ±0.57	-2.6 ±0.49	7.8 ±0.18	-2.7 ±0.16
$< \Delta\tau_{0.25} >$	z_0[ns]	ϵ_θ	z_0[ns]	ϵ_θ	z_0[ns]	ϵ_θ	z_0[ns]	ϵ_θ	z_0[ns]	ϵ_θ
$\log_{10} N_\mu^{tr}$	3.70 – 4.00		4.00 – 4.25		4.25 – 4.45		4.45 – 5.00		all N_μ^{tr}	
$40 < R_\mu[m] \leq 60$	3.1 ±0.12	-0.8 ±0.10	4.2 ±0.24	-1.4 ±0.21	4.7 ±0.46	-1.4 ±0.39	4.8 ±0.65	-1.4 ±0.57	2.4 ±0.05	-0.4 ±0.05
$60 < R_\mu[m] \leq 80$	3.3 ±0.12	-1.0 ±0.10	3.9 ±0.20	-1.2 ±0.17	3.9 ±0.39	-0.9 ±0.33	4.5 ±0.53	-1.1 ±0.46	2.9 ±0.06	-0.7 ±0.06
$80 < R_\mu[m] \leq 100$	3.5 ±0.13	-1.1 ±0.11	4.1 ±0.21	-1.5 ±0.18	4.6 ±0.48	-1.7 ±0.42	5.7 ±0.50	-2.1 ±0.42	3.3 ±0.08	-1.0 ±0.07
$100 < R_\mu[m] \leq 120$	4.2 ±0.18	-1.5 ±0.16	4.4 ±0.24	-1.5 ±0.21	4.7 ±0.44	-1.5 ±0.38	4.8 ±0.47	-1.4 ±0.40	4.1 ±0.12	-1.4 ±0.10
$< \Delta\tau_{0.75} >$	z_0[ns]	ϵ_θ	z_0[ns]	ϵ_θ	z_0[ns]	ϵ_θ	z_0[ns]	ϵ_θ	z_0[ns]	ϵ_θ
$\log_{10} N_\mu^{tr}$	3.70 – 4.00		4.00 – 4.25		4.25 – 4.45		4.45 – 5.00		all N_μ^{tr}	
$40 < R_\mu[m] \leq 60$	7.9 ±0.53	-2.3 ±0.47	8.6 ±0.47	-2.4 ±0.41	9.7 ±0.61	-3.1 ±0.52	9.9 ±0.74	-2.9 ±0.63	7.3 ±0.20	-1.9 ±0.18
$60 < R_\mu[m] \leq 80$	10.8 ±0.42	-4.1 ±0.36	11.1 ±0.79	-4.3 ±0.71	11.8 ±0.66	-4.5 ±0.56	12.3 ±0.75	-4.6 ±0.64	10.0 ±0.22	-3.7 ±0.19
$80 < R_\mu[m] \leq 100$	12.4 ±0.54	-4.8 ±0.45	12.2 ±0.81	-4.7 ±0.67	14.8 ±1.16	-6.7 ±1.01	14.4 ±0.83	-5.8 ±0.70	12.5 ±0.30	-5.0 ±0.25
$100 < R_\mu[m] \leq 120$	16.3 ±1.11	-7.3 ±1.00	16.5 ±0.88	-7.4 ±0.74	16.9 ±0.95	-7.7 ±0.78	17.2 ±1.03	-7.6 ±0.85	16.0 ±0.55	-7.1 ±0.49

Table 3: *The linear variation of* $T = z_0 + (\partial T/\partial \sec\theta) \mid_{N_\mu^{tr}} \cdot \sec\theta$ *for various time moments* T ($< \Delta\tau >, < \Delta\tau_{0.5} >, < \Delta\tau_{0.25} >, < \Delta\tau_{0.75} >$).